On the effect of multi-angle and spatially variable ground motions on cable-stayed bridges

Eleftheria Efthymiou[1], Alfredo Camara

[1]eefthymiou@smu.edu

Abstract

The definition of the Spatial Variability of the Ground Motion (SVGM) is a complex and multi-parametric problem. Its effect on the seismic response of long and multiply-supported structures in general, and on cable-stayed bridges, in particular, is important but not entirely understood. This work examines the effect of the SVGM on the seismic response of cable-stayed bridges by means of the time delay of the earthquake at different supports and of the loss of coherency of the seismic waves. The focus herein is the effect of the SVGM on cable-stayed bridges with various configurations in terms of their length and of design parameters, such as the pylon shape and the pylon–cable system configuration, combined with the influence of the incidence angle of the seismic waves. The aim of this paper is to provide general conclusions that are applicable to a wide range of cable-stayed bridges and to contribute to the ongoing effort to interpret and predict the effect of the SVGM. It has been found that the influence of the multi-support excitation on the seismic response of the bridges is strongly affected by the shape of the pylons, by the pylon–cable system configuration and by and the earthquake's incidence angle. It is also observed that the SVGM excites vibration modes of the bridges that do not contribute to their seismic response when identical support motion is considered.

1 Introduction

The Spatial Variability of the Ground Motion (SVGM) or multi-support excitation can be described by the differential movement of the supports of structures that are extended in length. Eurocode 8; Part 2 (2005) defines the SVGM in bridges as a '*situation in which the ground motion at different supports of the bridge differs and, hence, the seismic action cannot be based on the characterisation of the motion at a single point*'. According to Abdel-Ghaffar (1991), the multi-support excitation begins when the structure is long with respect to the wavelengths of the input motion in the frequency range of importance to its earthquake response and consequently, different supports may be subjected to different excitations.

The SVGM results from the combination of four components (Der Kiureghian and Neuenhofer 1992, Der Kiureghian 1996); the wave passage effect which refers to the difference in the arrival times of the ground motion to different stations; the incoherence effect which refers to the loss of coherency of the ground motion due to consequent reflections and refractions of the seismic waves in heterogeneous soil media; the site response effect which reflects the modification of the amplitudes and the frequency contents of the ground motions at different supports due to changes in the local site conditions; and the attenuation effect which describes the gradual decrease of the amplitudes of the seismic waves with distance as they travel away from the fault. The latter is not significant for the scale of bridges and can be neglected.

The effect of the SVGM on the structural response depends on a number of factors including the amplitude of the seismic motion, the incidence angle of the seismic waves relatively to the axis of the structure, the geometric characteristics of the structure and the stiffness of the surrounding soil.

This effect has been examined in different types of multiply-supported and long structures (Hindy and Novak 1980, Abdel-Ghaffar and Rubin 1983, Lee and Penzien 1983, Luco and Wong 1986, Hao *et al.* 1989, Zerva 1990, Abdel-Ghaffar and Nazmy 1991, Zerva 1991, Hao 1997, Shinozuka *et al.* 2000, Soyluk and Dumanoglu 2000, Tzanetos *et al.* 2000, Chen and Harichandran 2001, Allam and Datta 2004, Sextos *et al.* 2004, Soyluk and Dumanoglu 2004, Sextos and Kappos 2009, Bi *et al.* 2010, Sextos *et al.* 2014, Papadopoulos *et al.* 2017, among others) and it has been found that the SVGM induces differential movements among the supports of such structures which modify their seismic response (Hao *et al.* 1989). The multi-support excitation results in the decrease of the inertia-generated forces in a structure when compared to the forces resulting from the identical motion of the supports, and at the same time it generates pseudo-static forces that are not present when identical support motion is considered (Priestley *et al.* 1996).

The wave propagation velocity can influence significantly the effect of the SVGM on the response of a long structure. Typically lower values of the propagation velocity, c, tend to increase the structural response by increasing the pseudo-static forces induced under the SVGM and by decreasing their dynamic counterpart (Abdel-Ghaffar and Nazmy 1991, Zerva 1991, Soyluk and Dumanoglu 2000, Wang *et al.* 2003, Soyluk and Dumanoglu 2004, Bi *et al.* 2010). On the other hand, with increasing values of c the pseudo-static forces are reduced; and in the limit of an infinite value of the velocity of propagation ($c \to \infty$) the problem is reduced to the synchronous motion for which the pseudo-static effects are eliminated and the response is completely represented by the dynamic component (Soyluk and Dumanoglu 2000). Zerva (1991) investigated the impact of the incoherence and the wave passage effects on the response of multiply-supported structures by analysing two- and three-span continuous symmetric beams. The author concluded that the incoherence effect is more important than the wave passage effect, which can be neglected in cases where the seismic waves are highly incoherent. Shinozuka *et al.* (2000) verified that the incoherence effect is usually more important than the wave passage effect in typical highway bridges, but for longer spans, as the case of cable-stayed bridges, the time delay of the seismic motion at different supports may become critical. The specific site conditions at the deck articulation points of multiply-supported structures (site response effect) can modify the effect of the SVGM on the structure and in some cases this effect can prove critical to the seismic response (Der Kiureghian 1996). The impact of the differential motion of the supports on the overall seismic behaviour of the structure has been found to be beneficial when the supports are founded on stiff ground, whereas it is detrimental in the case of soft soil conditions (Mezouer *et al.* 2010). Generally, the more different the foundation sites among the different supports of long structures, the greater the effect of the SVGM on the seismic behavior (Ates *et al.* 2006), and usually the response is maximised when the structure resonates with the fundamental frequencies of the soil (Bi *et al.* 2010). The flexibility of the foundation can also affect the impact of the seismic waves on the structure. The SVGM is closely linked with the interaction of the foundation with the surrounding soil and the structure, most commonly referred to as soil–structure interaction or SSI (Lou and Zerva 2004, Sextos *et al.* 2004, Burdette *et al.* 2006).

The SVGM is more important on stiff structures and, typically, it does not significantly affect the response of longer and more flexible structures (Abdel-Ghaffar and Nazmy 1991, Nazmy and Abdel-Ghaffar 1992). The pseudo-static component of the structural response is responsible for the increased influence of the SVGM on stiff structures (Priestley *et al.* 1996, Zerva 2009), as opposed to flexible structures in which the total response is dominated by the dynamic component (Bi *et al.* 2010). This statement can be extended in the sense that the stiffer components of a structure such as a cable-stayed bridge that is composed of elements with very different flexibilities, are more vulnerable to the multi-support excitation. Similarly, the components that are controlled predominantly by higher-order modes are susceptible to the effect of the SVGM because the pseudo-static response becomes important in lower frequencies (Abdel-Ghaffar and Nazmy 1991, Nazmy and Abdel-Ghaffar 1992, Soyluk and Dumanoglu 2004, Sextos and Kappos 2008). The SVGM is reportedly responsible for the increased contribution of higher-order and mainly antisymmetric vibration modes to the structural response (Tzanetos *et al.* 2000, Sextos 2001). In other words, symmetric structures do not behave symmetrically when subjected to multi-support excitations. In fact, in a symmetric structure the SVGM may excite antisymmetric modes (Zerva 2009) which do not contribute to the structural response of the bridge when identical support excitation is considered, suggesting that the SVGM has a fundamentally different effect on structures from a vibrational viewpoint (Sextos *et al.* 2014, Camara and Efthymiou 2016, Papadopoulos and Sextos 2018).

Finally, the combination of the incidence angle with the SVGM has started to gain the attention of the research community, with different works stating that the maximum value of the response quantity under consideration may not occur when the direction of propagation coincides with the principal axes of the bridge. Specifically, Allam and Datta (2004) and more recently Khan (2012) examined a 335-m span cable-stayed bridge with different orientations with respect to the propagation of the earthquake and subjected to ground motions whose rate of correlation depended on the incidence angle of the seismic waves. The authors observed that there existed critical orientations of the examined bridge, which depended on the response quantity of interest and the region of the bridge under consideration, in which the structural response was larger than the obtained one when the ground motion coincided with the principal directions of the bridge.

The objective of this paper is to provide practical conclusions that are applicable to a wide range of cable-stayed bridges and to interpret and predict the effect of the SVGM based on different design considerations. From the dynamic analysis of a large number of cable-stayed bridges with different configurations that are subjected to multi-angle and spatially variable ground motions it has been observed that the influence of the multi-support excitation on the seismic response of the bridges is strongly affected by the shape of the pylons, the pylon–cable system configuration and by the incidence angle of the seismic waves. The SVGM also excites vibration modes that do not contribute to the seismic response of the pylons when identical support motion is considered.

2 Numerical Models

The bridge models employed in this study are based on previous works from Camara (2011), Camara *et al.* (2014) and Efthymiou and Camara (2015). The overall arrangement in each bridge model consists of two symmetric reinforced concrete pylons, a composite deck and the cable system. The length, L_P, of the span between the centres of the two pylons takes values of 200, 400 and 600 m, representing short-span, intermediate-span and relatively long-span cable-stayed bridges, respectively. Pylons with conventional 'H'-, inverted 'Y'- and 'A'- shapes have been considered. A diamond configuration has also been examined in the lower part of the pylons of inverted 'Y' and 'A' shapes, as shown in Fig. 1 wherein the notation of the pylons is also included and will be followed hereinafter. Altogether 21 bridge models have been considered.

The length of the main span, L_P, defines the length of the side spans, L_S, as shown in Fig. 2, and also the number of cables, N_T, in each plane; $N_T = 9$, 19 and 29 when $L_P = 200$, 400 and 600 m, respectively. The height of the pylons above the deck level, H, is defined as a function of L_P; $H = L_P/4.8$ and it is the same for all the pylon shapes. Below the deck the height of the pylons is $H_i = H/2$, leading to the total height of the pylons being $H_{tot} = H + H_i = 62.5$, 125 and 187.5 m for the 200-, 400- and 600-m main span bridges, respectively. The heights of the different regions of the pylons along with the section dimensions of the legs and the transverse struts of the pylons are defined as functions of the height, H (Camara *et al.* 2014).

The cables are arranged in a semi-harp configuration in the orientation parallel to the traffic, whereas in the transverse direction two different configurations have been employed; the case of two lateral cable planes (LCP) for all the pylon geometries and one central cable plane (CCP) only in the

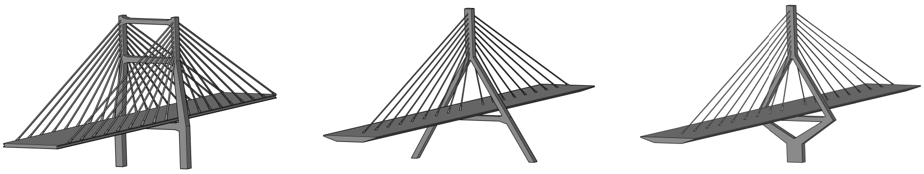

(a) H-LCP (b) Y-CCP (c) YD-CCP

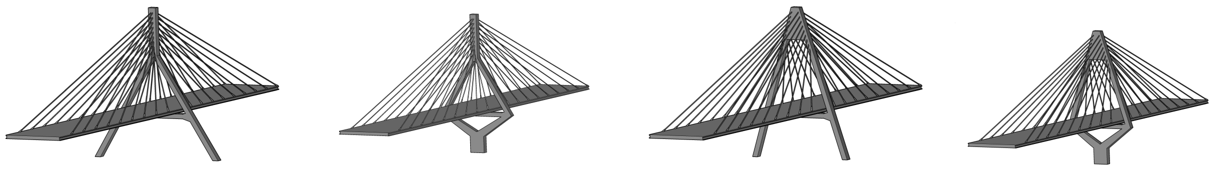

(d) Y-LCP (e) YD-LCP (f) A-LCP (g) AD-LCP

Figure 1: Different pylon shapes and cable system arrangements considered in this work, along with the reference keywords. The part of the notation before the hyphen corresponds to the shape of the pylon. The letter 'D' stands for the lower diamond configuration which has been considered in the inverted 'Y'- and 'A'-shaped pylons. The cable arrangement is included in the second part of the notation after the hyphen and dictates two lateral cable planes (LCP) or one central cable plane (CCP).

inverted 'Y'-shaped pylon with and without the lower diamond. Two different deck sections have been examined whose shape is associated with each cable system configuration. In the case of two LCP's the deck has an open section, as opposed to adopting a closed box section when one CCP is selected. The width of the deck is 25 m to accommodate four traffic lanes, regardless of the length of the bridge. In LCP bridges the deck has an open composite cross-section formed of two longitudinal I-shaped steel girders at the edges and a 25-cm thick concrete slab on top. To ensure the overall stability of the deck, transverse I-beams connecting the two longitudinal girders are placed at fixed intervals. In CCP bridges the deck is a composite box girder that provides the bridge with sufficient torsional rigidity by means of a steel U-section closed by a 25-cm thick concrete slab. The composite box section is stiffened with transverse steel diaphragms at the same fixed intervals as in the open deck section of the bridges with two LCP's. In the side spans vertical piers are placed at a distance of L_{IP} from the abutments that constrain the vertical displacement of the deck in order to control the longitudinal displacement of the upper part of the pylon where the cable system is anchored (see Fig. 2).

Figure 2 shows that the abutments constrain the displacements of the deck in the vertical (z), transverse (y–perpendicular to the traffic flow) and longitudinal (x) directions and they also prevent its torsional rotation (θ_{xx}), whereas the rotations around the transverse (θ_{yy}) and the vertical axis (θ_{zz}) are released. In the side spans the intermediate piers constrain the vertical displacement and the torsional rotation of the deck. At the pylons the deck is restrained in the y direction and it is released in all other directions, assuming a floating type connection between the deck and the pylon which is commonly adopted in the design of cable-stayed bridges in seismic prone regions. The SSI is considered in this work by replacing the soil around the foundation of the pylons with a system of springs and dashpots whose stiffness and damping properties are obtained from Gazetas (1991). The dynamic impedances are computed for the movement in the three principal directions of the bridge (x–traffic, y and z) and for the rotation around the x and y axes (θ_{xx} and θ_{yy}, respectively). The spring–dashpot systems have constant properties which are calibrated to the mean frequency of the earthquake, f_m (Málaga-Chuquitaype and Elghazouli 2012, Stefanidou *et al.* 2017, Demirci *et al.* 2018).

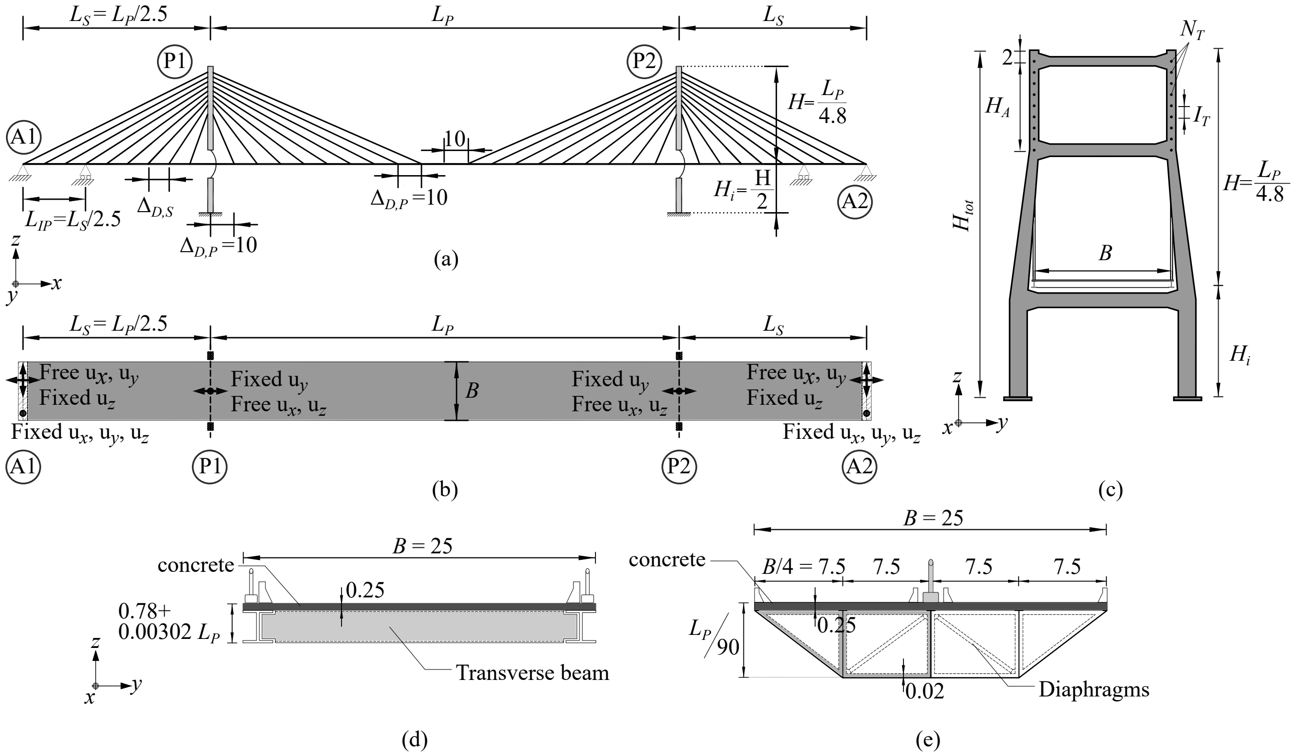

Figure 2: Parametric definition of the cable-stayed bridge models. (a) Complete bridge elevation, (b) complete bridge plan view, (c) sample 'H'-shaped pylon (the same parametrisation rules are applied to the inverted 'Y'- and 'A'-shaped pylons), (d) LCP deck, (e) CCP deck. All dimensions are in [m].

The materials (steel and concrete) that are used in the cable-stayed bridges are described through their constitutive models. The material properties have been selected following the suggestions of international codes of practice; Eurocode 2; Part 1.1 (2004), Eurocode 3; Part 1.1 (2005), Eurocode 3; Part 1.11 (2006), Eurocode 8; Part 2 (2005). The concrete used in the pylons is C40 concrete with Young's modulus $E_c = 35$ GPa and density $\rho_c = 2500$ kg/m^3. The structural steel in the deck sections is B500C grade with $E_s = 210$ GPa and $\rho_s = 7850$ kg/m^3, while for the prestressing steel forming the cables the Young's modulus is $E_p = 190$ GPa. The structural damping in the dynamic analysis is described by means of Rayleigh's damping theory with a target damping of 2% to account for the low structural dissipation that characterises the elastic response of cable-stayed bridges (Kawashima *et al.* 1993) and it is independent of the material (concrete or steel).

The finite element (FE) analysis software Abaqus (2018) has been used to model the bridges and to conduct the complete sets of dynamic analyses. Figure 3 shows that the deck sections of the LCP and CCP models are discretised with linear interpolation, shear-flexible beam-type elements that pass through the centre of gravity of the sections and account for the structural (reinforced concrete slab, longitudinal and transverse steel girders and steel diaphragms) and nonstructural (deck asphalt) masses, as shown in Figs. 3(b) and 3(c). Lump mass elements located at both cable ends represent the anchorage masses which, at the deck end of each cable, also include the parapets in the deck. The pylons are also modelled with beam-type elements through the centre of gravity of their sections (see Fig. 3(d)). The cables are modelled with 3D trusses which use linear interpolation of the axial displacements. Each truss element represents one cable, ignoring the cable-structure interaction (Efthymiou and Camara 2015).

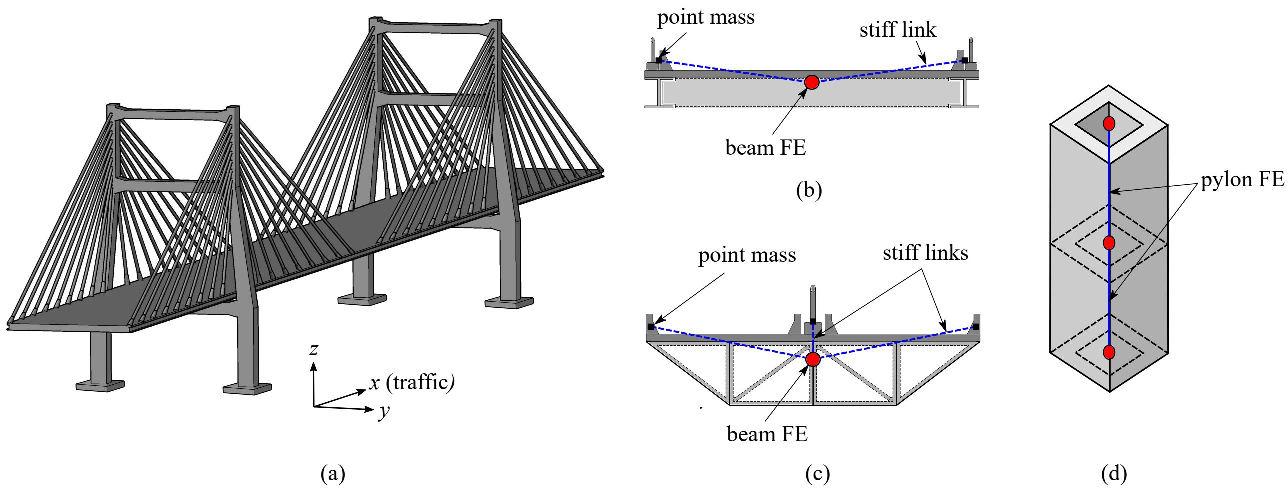

Figure 3: (a) Complete 3D model of the H-LCP model with $L_P = 200$ m, (b) FE model of the LCP deck, (c) FE model of the CCP deck and (d) FE model of the pylon.

3 Seismic Action

For this work artificial sets of accelerograms have been generated based on the Eurocode 8; Part 1 (2004) elastic response spectrum with 2% damping. The target spectrum is defined for two extremely different sites corresponding to ground categories A and D. Those were modified by a coherency model to account for the loss of coherency between the accelerograms at different supports of the bridges. Various coherency models were examined by Efthymiou and Camara (2017) and the one by Harichandran and Vanmarcke (1986), which considers incoherent seismic waves in low frequencies that are important to the seismic response of cable-stayed bridges, was the most appropriate for this work. This model describes the coherency between the signals at two different stations m and n as:

$$|\gamma(l_{mn},f)| = A\exp\left[\frac{-2B_{\mathrm{HV}}l_{mn}}{a_{\mathrm{HV}}\nu(f)}\right] + (1-A)\exp\left[\frac{-2B_{\mathrm{HV}}l_{mn}}{\nu(f)}\right] \tag{1}$$

$$\nu(f) = k\left[1+\left(\frac{f}{f_0}\right)^b\right]^{-1/2} \quad \text{and} \quad B_{\mathrm{HV}} = (1-A+a_{\mathrm{HV}}A)$$

where: l_{mn} is the separation distance between stations m and n, f is the frequency and $\nu(f)$ is the frequency-dependent spatial scale of fluctuation. The values of the model parameters were defined as:

$$A = 0.736; \quad a_{\mathrm{HV}} = 0.147; \quad k = 5120 \text{ m}; \quad f_0 = 1.09 \text{ Hz}; \quad b = 2.78$$

For the generation of spectrum-compatible acceleration histories the methodology proposed by Deodatis (1996) has been adopted. Based on the assumption that stochastic processes can be described as a sum of cosine functions with random phase angles (Shinozuka 1972), the representation of a homogeneous Gaussian random process $f(x)$ with zero mean and standard deviation $\sqrt{2\,S(\omega)\Delta\omega}$ can be described as:

$$f(t) = \sqrt{2}\sum_{i=1}^{K} C_k\cos(\omega_k t + \phi_k) \tag{2}$$

where $C_k = \sqrt{2S(\omega_k)\Delta\omega}$, S is the power spectral density (PSD), ω_k with $k = 1, 2, \ldots, K$ is the discrete circular frequency, $\Delta\omega$ is the frequency step and ϕ_k are independent random phase angles uniformly distributed over the range $[0, 2\pi)$. The accelerograms are considered to be non-stationary processes, but the strong motion window of the time-histories can be viewed as a stationary process (Harichandran and Vanmarcke 1986), hence for the generation of stationary acceleration time-histories the following methodology applies.

When considering multivariate, stationary stochastic processes with zero mean, the cross spectral density matrix is given as a function of the circular frequency ω [rad/s]:

$$S(\omega)=\begin{bmatrix} S_{11}(\omega) & S_{12}(\omega) & \dots & S_{1m}(\omega) \\ S_{21}(\omega) & S_{22}(\omega) & \dots & S_{2m}(\omega) \\ \vdots & \vdots & \ddots & \vdots \\ S_{m1}(\omega) & S_{m2}(\omega) & \dots & S_{mm}(\omega) \end{bmatrix} \tag{3}$$

where m is the number of stations, S_{jj} is the PSD of the motion at station j with $j=1,2,\dots,m$, S_{jk} is the cross spectral density between stations j and k with $j,k=1,2,\dots,m$, and $j\neq k$, $S_{jk}(\omega)=\sqrt{S_{jj}(\omega)S_{kk}(\omega)}\gamma_{jk}(\omega)$ and $\gamma_{jk}(\omega)$ is the complex coherency function between stations j and k

$$\gamma_{jk}(\omega)=\frac{S_{jk}(\omega)}{\sqrt{S_{jj}(\omega)S_{kk}(\omega)}} \tag{4}$$

Based on the theory of evolutionary spectra (Priestley 1965), one can consider a nonstationary process of time and frequency by means of a modulating function, $I_{j(k)}(\omega,t)$, as follows:

$$S_{jj}(\omega,t)=|I_j(\omega,t)|^2 S_{jj}(\omega) \tag{5a}$$

$$S_{jk}(\omega,t)=I_j(\omega,t)I_k(\omega,t)S_{jk}(\omega) \tag{5b}$$

For the resulting nonstationary process the cross spectral density matrix becomes a function of ω and the time t:

$$S(\omega,t)=\begin{bmatrix} S_{11}(\omega,t) & S_{12}(\omega,t) & \dots & S_{1m}(\omega,t) \\ S_{21}(\omega,t) & S_{22}(\omega,t) & \dots & S_{2m}(\omega,t) \\ \vdots & \vdots & \ddots & \vdots \\ S_{m1}(\omega,t) & S_{m2}(\omega,t) & \dots & S_{mm}(\omega,t) \end{bmatrix} \tag{6}$$

The matrix is Hermitian and its elements have the following properties:

$$S_{jj}(\omega,t)=S_{jj}(-\omega,t), \quad j=1,2,\dots,m \tag{7a}$$

$$S_{jk}(\omega,t)=S^{*}_{jk}(-\omega,t), \quad j,k=1,2,\dots,m \text{ and } \quad j\neq k \text{ for every } t \tag{7b}$$

$$S_{jk}(\omega,t)=S^{*}_{jk}(\omega,t), \quad j,k=1,2,\dots,m \text{ and } \quad j\neq k \text{ for every } t \tag{7c}$$

where the symbol * denotes the complex conjugate of a number. The matrix in Eq. (6) can be decomposed at every time instant t into the following:

$$S(\omega,t)=H(\omega,t)H^{\mathrm{T}*}(\omega,t) \tag{8}$$

where the symbol $^{\mathrm{T}}$ denotes the transpose of a matrix. The decomposition can be performed by means of the Cholesky method in which case $H(\omega,t)$ is a lower triangular matrix:

$$H(\omega,t)=\begin{bmatrix} H_{11}(\omega,t) & 0 & \dots & 0 \\ H_{21}(\omega,t) & H_{22}(\omega,t) & \dots & 0 \\ \vdots & \vdots & \ddots & \vdots \\ H_{m1}(\omega,t) & H_{m2}(\omega,t) & \dots & H_{mm}(\omega,t) \end{bmatrix} \tag{9}$$

where $H_{jj}(\omega, t)$ are real, non-negative values and $H_{jk}(\omega, t)$ with $j,\ k = 1,\ 2, \ldots,\ m$ and $j \neq k$ are complex functions of the circular frequency ω and of time t. H_{jk} can be re-written in polar form as follows:

$$H_{jk}(\omega, t) = |H_{jk}(\omega, t)| \exp\left[\mathrm{i}\,\theta_{jk}(\omega, t)\right] \quad \text{with} \quad \theta_{jk} = \tan^{-1}\frac{\mathrm{Im}\left[H_{jk}(\omega, t)\right]}{\mathrm{Re}\left[H_{jk}(\omega, t)\right]} \tag{10}$$

Finally, having decomposed the cross spectral density matrix $S_{jk}(\omega, t)$, the spectrum-compatible acceleration history at the j^{th} support of the bridge is extended from Eq. (2):

$$f_j(t) = 2\sum_{m=1}^{4}\sum_{l=1}^{N}\left|H_{jm}(\omega_l, t)\right|\sqrt{\Delta\omega}\cos\left(\omega_l t - \theta_{jm}(\omega_l, t) + \Phi_{ml}\right) \quad \text{with} \quad j = 1, 2, 3, 4 \tag{11}$$

where j represents the support of interest and m the total number of supports between which the stochastic process is established. Herein, the simulation of the SVGM starts with the first abutment ($m = 1$) and continues with the first pylon ($m = 2$), the second pylon ($m = 3$) and the second abutment ($m = 4$). $\omega_l = l\Delta\omega$ (with $l = 1, 2, \ldots, N$) is the discrete frequency, $\Delta\omega = \omega_u/N$ is the frequency step, ω_u is the cut-off frequency beyond which the cross spectral density matrix has practically no effect on the simulations, Φ_{ml} are independent random phase angles uniformly distributed over the range $[0, 2\pi)$.

Deodatis (1996) proposed an iterative scheme. By initially introducing $S_{jj}(\omega)$ as constant noise for the whole frequency range, stationary histories are generated based on Eq. (11). The resulting stationary signals are consequently modulated by appropriately selected functions, $I(\omega, t)$, to become non-stationary processes $\ddot{u}_{g,\,j}(t)$ with $j = 1, 2, 3, 4$ corresponding to the four supports of the bridge, as described above. For the seismic signals of this study, uniformly modulated stochastic processes have been considered and hence the modulating function is reduced to a function of time only; $I(\omega, t) = I(t)$ and hence

$$\ddot{u}_{g,\,j}(t) = I(t) f_j(t) \tag{12}$$

The stationary signals obtained from Eq. (11) are modulated in time to be assigned a finite total duration and a strong motion window (Amin and Ang 1966, Jennings *et al.* 1968):

$$I(t) = \begin{cases} \left(\frac{t}{t_1}\right)^2 & \text{if } 0 \leq t < t_1 \\ 1 & \text{if } t_1 \leq t < t_2 \\ \exp\left[-\mathrm{c}_m(t - t_1)\right] & \text{if } t \geq t_2 \end{cases} \tag{13}$$

The strong motion window of this intensity modulating function preserves the target PGA of the stationary signal i.e. $I(t) = 1$ if $t_1 \leq t \leq t_2$. The values for the modulating function are:

$$t_1 = 1.5\ \mathrm{s}; \quad t_2 = 9\ \mathrm{s}; \quad \mathrm{c}_m = 0.4\ \mathrm{s}^{-1}$$

The non-stationary acceleration history at support j from the i^{th} iteration, $\ddot{u}^{(i)}_{g,\,j}(t)$, is obtained and subsequently, the response spectrum of $\ddot{u}^{(i)}_{g,\,j}(t)$, $\mathrm{RS}^{(i)}_j$, is compared to the target $\mathrm{RS}^{\text{target}}_j$ and the process is repeated with an updated S_{jj} until acceptable convergence is reached, as follows:

$$S^{(i+1)}_{jj}(\omega) = \left[\frac{\mathrm{RS}^{\text{target}}_j(\omega)}{\mathrm{RS}^{(i)}_j(\omega)}\right]^2 S^{(i)}_{jj}(\omega) \tag{14}$$

where: $S^{(i+1)}_{jj}$ is the resulting PSD at station j for the next iteration.

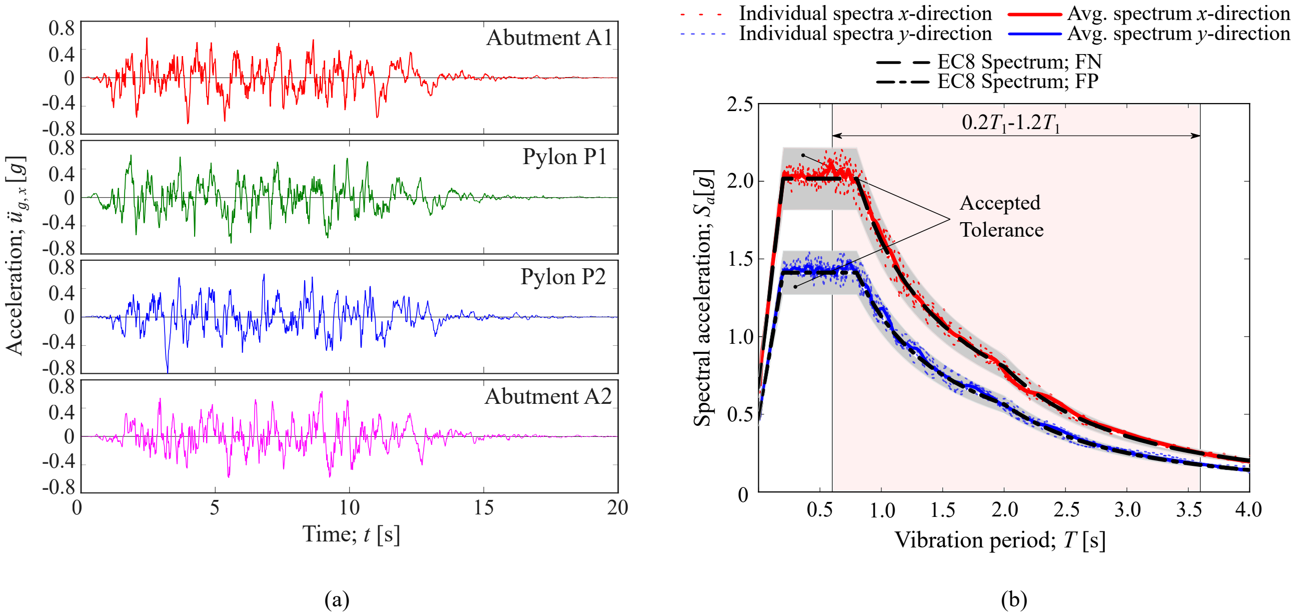

Figure 4: (a) Sample set of acceleration histories corresponding to the FN earthquake component when c =1000 m/s, (b) average (Avg.) of the acceleration spectra at the four supports of the bridge. The target spectra are also included. L_P = 400 m.

The cutoff frequency, ω_u, that defines the frequency step, $\Delta\omega$, is taken as 220 rad/s (f_u = 35 Hz) because beyond this limit the contribution of the vibration frequencies to the response is not of interest in most structures (Chopra 2017). The lower limit of the frequency range, $\omega_{\min}$, is defined by the fundamental frequency of the structure. The range of important periods is taken as [$0.2T_1$, $1.2T_1$] in the seismic analysis of cable-stayed bridges, T_1 being the fundamental vibration period of the structure, based on findings from Camara (2011). The frequency step is $\Delta\omega = 0.5$ rad/s and the frequency parameters for the bridges with L_P = 200, 400 and 600 m are summarized in the following:

$$\omega_u = 220 \text{ rad/s } (f_u = 35 \text{ Hz}); \quad \Delta\omega = 0.5 \text{ rad/s}$$

$$\omega_{\min,200} = 2.62 \text{ rad/s}; \quad \omega_{\min,400} = 1.75 \text{ rad/s}; \quad \omega_{\min,600} = 1.05 \text{ rad/s};$$

Apart from the loss of coherency, this study also accounts for the temporal variability of the ground motion by means of the delay between the arrival times of the seismic waves at neighbouring supports, which can reach several seconds in long structures such as cable-stayed bridges (Soyluk and Dumanoglu 2000). The reference support is the first abutment (A1) which is affected by the earthquake at time instance t_{A1} = 0 s and then the ground motion propagates parallel to the deck with velocity of propagation c = 1000 m/s. Table 1 includes the time instances when the earthquake reaches each support calculated on the basis of the different span lengths.

Table 1: Time instances t_j with j = A1, P1, P2, A2 of the arrival of the seismic waves at different supports of the cable-stayed bridges depending on the main span length L_P. t_j in [s].

L_P = 200 m				L_P = 400 m				L_P = 600 m			
t_{A1}	t_{P1}	t_{P2}	t_{A2}	t_{A1}	t_{P1}	t_{P2}	t_{A2}	t_{A1}	t_{P1}	t_{P2}	t_{A2}
0	0.08	0.28	0.36	0	0.16	0.56	0.72	0	0.24	0.84	1.08

The effect of the SVGM on the seismic response of cable-stayed bridges is illustrated by comparing the response quantity of interest from the SVGM to the respective quantity from the identical support motion i.e. when considering infinite velocity of the seismic waves. This case is referred to as the synchronous motion scenario (SYNC), in which the reference action at the abutment A1 is applied to the four supports of the cable-stayed bridges simultaneously. To explore the effect of the local site conditions at the supports (i.e. site response effect), two extremely different ground categories are examined between the abutments and the pylons, corresponding to rocky ground type A (as defined in Eurocode 8; Part 1 (2004)) at the abutments and soft soil type D at the pylons.

Seven sets of spectrum-compatible acceleration histories have been generated parallel to the two horizontal components of the seismic action, namely 'Fault Parallel' (FP) and 'Fault Normal' (FN), the latter coinciding with the direction of wave propagation. For the generation of the accelerograms corresponding to the FP component of the motion the target spectrum is reduced to 70% to account for the principal components of the earthquake (Lopez *et al.* 2006). The coherency has been assumed independent of the direction of propagation, allowing for the same loss of coherency model to be used for the generation of signals corresponding to the FN and FP components (Sextos *et al.* 2003). The resulting accelerograms are considered acceptable when the obtained RS of each signal falls within the range 90%-110% of the target spectrum in the range of important periods of the studied bridges: $[0.2T_1, 1.2T_1]$, T_1 being the fundamental vibration period of the structure in each case (Camara 2011). Considering the seven different structural typologies, T_1 is 2.0, 2.87 and 5.09 s on average when $L_P =$ 200, 400 and 600 m, respectively. An indicative set of accelerograms generated for the supports of the 400-m main span bridge is included in Fig. 4(a), where the time delay and the loss of coherency between supports can be appreciated. The generated sets of accelerograms have been corrected to remove the baseline drift at the end of the displacement time-histories. Figure 4(b) shows a good match between the FN and FP target spectra and those of the resulting signals.

In order to explore the effect of the angle of incidence of the seismic waves, the bridges are rotated in the range of [0°, 180°] with increments of 30°. This work adopts the interpretation of the incidence angle of the earthquake from Mackie *et al.* (2011). This is illustrated in Fig. 5 which shows that the axis of the bridge forms an angle θ with the FN component of the earthquake. When $\theta = 0°$ the FN earthquake component coincides with the bridge axis and when $\theta = 90°$ the bridge is rotated clockwise so that the FP component of the earthquake is parallel to the bridge axis. The different orientations of the bridge considered in this work are shown in Fig. 6. In the intermediate angles of incidence, the accelerograms are projected to the local x (bridge axis) and y axes of the bridge by means of the rotation matrix:

$$\begin{pmatrix} \ddot{u}_{g,x} \\ \ddot{u}_{g,y} \end{pmatrix} = \begin{pmatrix} \cos\theta & \sin\theta \\ \sin\theta & -\cos\theta \end{pmatrix} \begin{pmatrix} \ddot{u}_{g,\mathrm{FN}} \\ \ddot{u}_{g,\mathrm{FP}} \end{pmatrix} \tag{15}$$

where $\ddot{u}_{g,x}$ and $\ddot{u}_{g,y}$ are the accelerations corresponding to the x and y axes of the bridge and $\ddot{u}_{g,\mathrm{FN}}$ and $\ddot{u}_{g,\mathrm{FP}}$ are the accelerations corresponding to the FN and FP components of the earthquake, respectively. The rotation of the incoherent and delayed ground motions is presented in Fig. 5.

4 Analysis and Results

The complete set of bridges have been analyzed by means of the direct response history analysis, assuming that the constituent materials behave in a linear elastic manner during the seismic excitation. The geometric nonlinearities arising from the large deformations, a characteristic of cable-stayed bridges (Abdel-Ghaffar and Nazmy 1991), have been accounted for in the analysis. The results of the analyses are presented in terms of the arithmetic mean (μ) of the peak seismic axial load (N), the longitudinal shear force (V_x) and the transverse shear force (V_y) along the pylon legs.

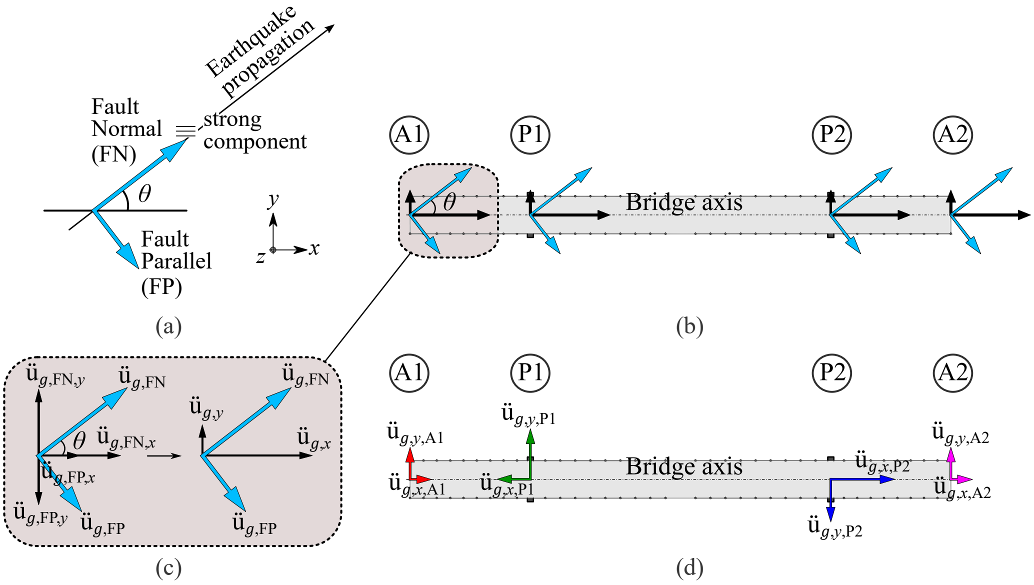

Figure 5: Incidence angle of the seismic waves with respect to the axis of the bridge; (a) principal components of the earthquake, (b) incidence angle θ of the seismic waves and corresponding projected earthquake components (black lines) in the case of synchronous motion of the supports and (c) detailed projection of the principal earthquake components to the local x and y axes of the bridge (*following from (b)*), (d) projected earthquakes $\ddot{u}_{g,\,i,\,j}$, with $i = x$, y and $j =$ A1, P1, P2, A2 at time instance t from the start of the earthquake and for a given coherency γ.

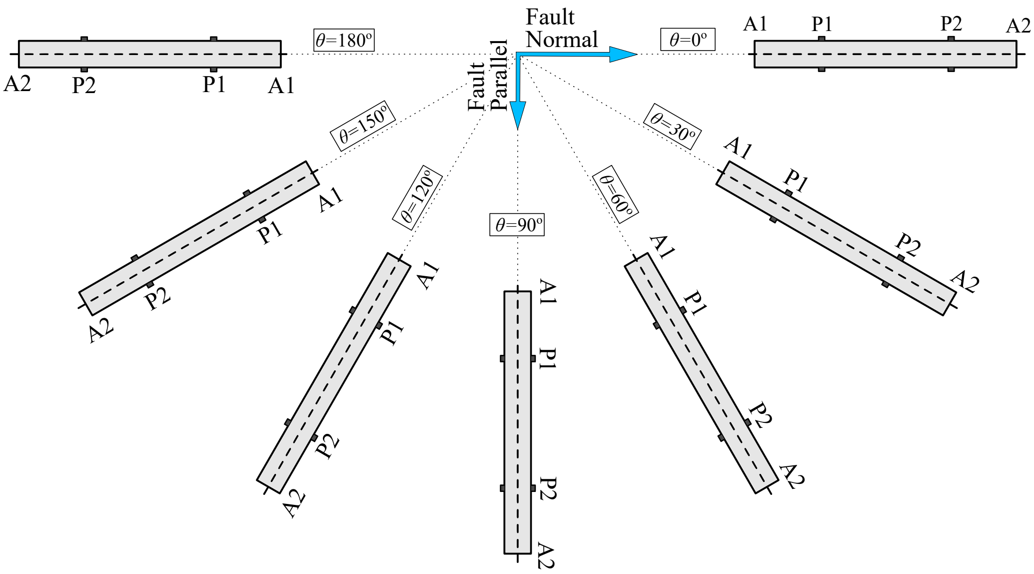

Figure 6: Rotation of the bridge to examine the effect of the angle of incidence of the seismic waves in the range [0°, 180°] with 30° increments.

4.1 Effect of the Foundation Site Conditions

This section explores the influence of the foundation site on the seismic response and of the lack of uniformity among the foundation sites at the abutments and the pylons. Specifically, three different scenarios are examined for the H-LCP model with $L_P = 400$ m when the strong component of the earthquake (FN) is applied parallel to the deck (i.e. $\theta = 0°$). The case of uniform ground conditions at the four supports is considered for rocky ground corresponding to type A of Eurocode 8; Part 1 (2004) and referred to as AAAA hereinafter, and for soft soil corresponding to type D (i.e. DDDD). The site response effect (referred to as 'sr' in the notation) is examined by considering a case of nonuniform foundation sites at the supports which corresponds to ground category A under the two abutments of

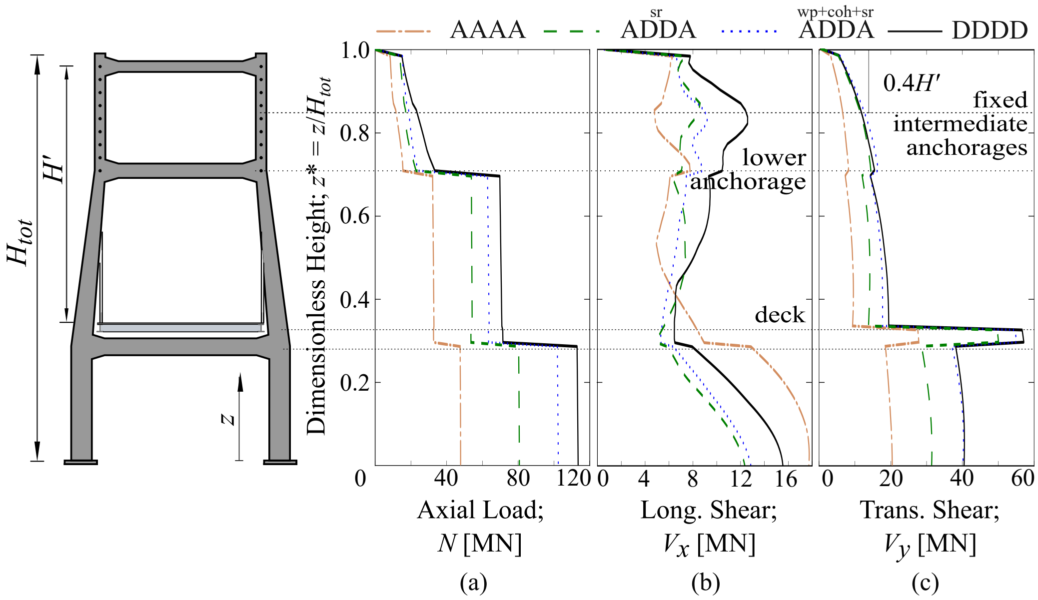

Figure 7: Influence of the foundation ground type under the different supports of the cable-stayed bridge on (a) the peak seismic axial force N, (b) the longitudinal shear force V_x and (c) the transverse shear force V_y. H-LCP model with $L_P = 400$ m; $\theta = 0°$, $c = 1000$ m/s. 'A' and 'D' denote the respective ground categories of Eurocode 8; Part 1 (2004) at the foundations of the supports, 'wp' stands for wave passage, 'coh' for incoherence and 'sr' stands for the site response components of the SVGM.

each cable-stayed bridge and ground category D under the two pylons (ADDA). In addition, two different scenarios are examined to examine the effect of the SVGM. In the first scenario the nonuniform foundation sites are examined alone, without the loss of coherency (referred to as 'coh') and the wave passage ('wp') components of the SVGM, in order to isolate the effect of the foundation site on the seismic response, whereas in the second scenario the effects of the three components are combined (i.e. 'wp+coh+sr').

Figure 7 presents the peak seismic response along the height of the pylon in the vertical, longitudinal and transverse directions of the bridge by means of the seismic forces developed in the pylon (N, V_x and V_y, respectively). The two cases of uniform sites are generally associated with the lowest (AAAA) and the highest (DDDD) seismic responses in the part of the pylon above the deck level. The maximum response is obtained at the base of the pylon, where the axial load and the longitudinal shear force are examined in Fig. 7(a),(b), respectively, and at the level of the deck in the transverse direction of the response in Fig. 7(c) due to the lateral deck-pylon reaction. When the DDDD scenario is considered there is an increase of 135%, a reduction of 14% and an increase of 104% in the peak values of N_{base}, $V_{x,\text{base}}$ and $V_{y,\text{deck}}$, respectively, compared to the peak values responses obtained from scenario AAAA. The increments in N and V_y are due to the higher spectral acceleration that is associated with dominant vibration modes of the structures when ground type D is considered compared to the respective accelerations of the ground type A spectrum. Figure 8 shows that the fundamental vibration mode of the 400-m main span bridge, which involves the vertical flexure of the deck combined with the longitudinal flexure of the pylons in opposite directions, and the first transverse mode of the bridge, which involves the transverse flexure of the deck and the pylons, are associated with higher spectral accelerations ($S_{a,\text{D}}^{T_x}$ and $S_{a,\text{D}}^{T_y}$, respectively) than the respective ones for ground type A ($S_{a,\text{A}}^{T_x}$ and and $S_{a,\text{A}}^{T_y}$, respectively). The effect of the soft soil conditions is also noticed at the anchorage area of the pylon in the longitudinal response in which there is an increase of 150% in V_x compared to the response when ground type A is considered at the foundation of the four supports. This is attributed to the longitudinal restraint introduced by the cables anchored to the abutments and to the vertical piers in the side spans, which gains importance due to the increment of $S_{a,\text{D}}^{T_x}$.

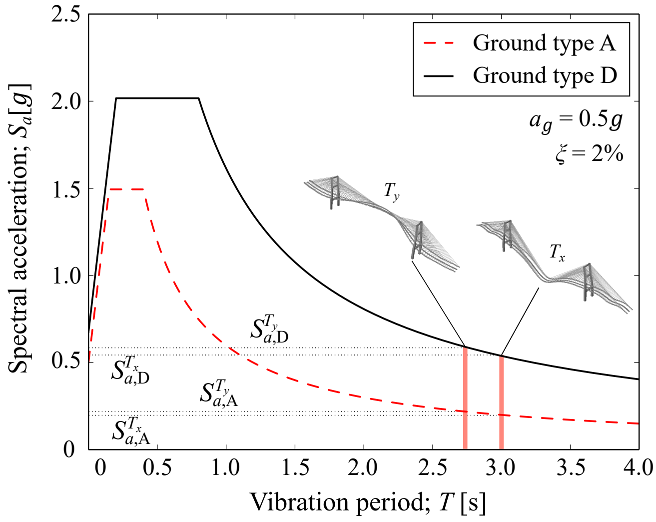

Figure 8: Eurocode 8; Part 1 (2004) Type 1 elastic response spectra for ground categories A and D with $a_g = 0.5g$ and $\xi = 2\%$. Longitudinal and transverse vibration modes of the cable-stayed bridge with 'H'-shaped pylons and $L_P = 400$ m.

When nonuniform soil conditions are considered (ADDA) the seismic response generally falls within the limits defined by AAAA and DDDD. Lower values of V_x are obtained below the deck level down to the base of the pylon legs in which the peak longitudinal shear force is 23% smaller than the longitudinal response from the DDDD ground scenario. The similar longitudinal response at the base of the pylons in the two cases with nonuniform sites is associated with the SSI which is relevant when soft soil of category D is considered. It is noticed in Fig.7(b) that when the SSI is accounted for at the foundations of the pylons (i.e. in ADDA and DDDD cases) V_x is reduced compared to the respective shear force when the pylons are founded on rock and the ssi is not considered (i.e. fixed base). The flexibility of the foundation in the ADDA and DDDD scenarios compensates for the increased seismic forces resulting from the higher spectral acceleration when soil type D is considered compared to ground type A. Finally, when the three components of the SVGM are combined (i.e. $\overset{\text{wp+coh+sr}}{\text{ADDA}}$) the vertical, longitudinal and transverse responses of the pylon, in almost all its height, are larger than the responses when only the local site conditions are considered alone (i.e. $\overset{\text{sr}}{\text{ADDA}}$).

4.2 Multi-Angle Response

Asymmetry of the Response

The apparent symmetry of the structures described in Section 2 is lost in the seismic response for different incidence angles (θ) due to: (1) the lack of symmetry of the support conditions at the abutments A1 and A2 with respect to the centreline of the deck (axis x), as shown in Fig. 2; (2) the longitudinal movement of the deck during the earthquake, which introduces axial compression in one pylon and tension in the opposite due to the effect of the cable system; and (3) the difference in the ground motion at different supports due to the loss of coherency and the time lag from the SVGM (Fig. 5(d)). The objective of this section is to explore the effect of this asymmetry on the seismic response.

Figure 9 shows the arithmetic mean of V_x and V_y along the pylons under the SVGM and the SYNC motion when the strong earthquake component (FN) is considered parallel to the deck of the bridge but with different signs: $\theta = 0°$ and $\theta = 180°$. The effect of the asymmetry of the response is reflected in this figure by comparing the seismic shear forces in pylon P1 when $\theta = 0°$ with the response of P2 when $\theta = 0°$. It is observed that the asymmetry of the response is relevant in the longitudinal

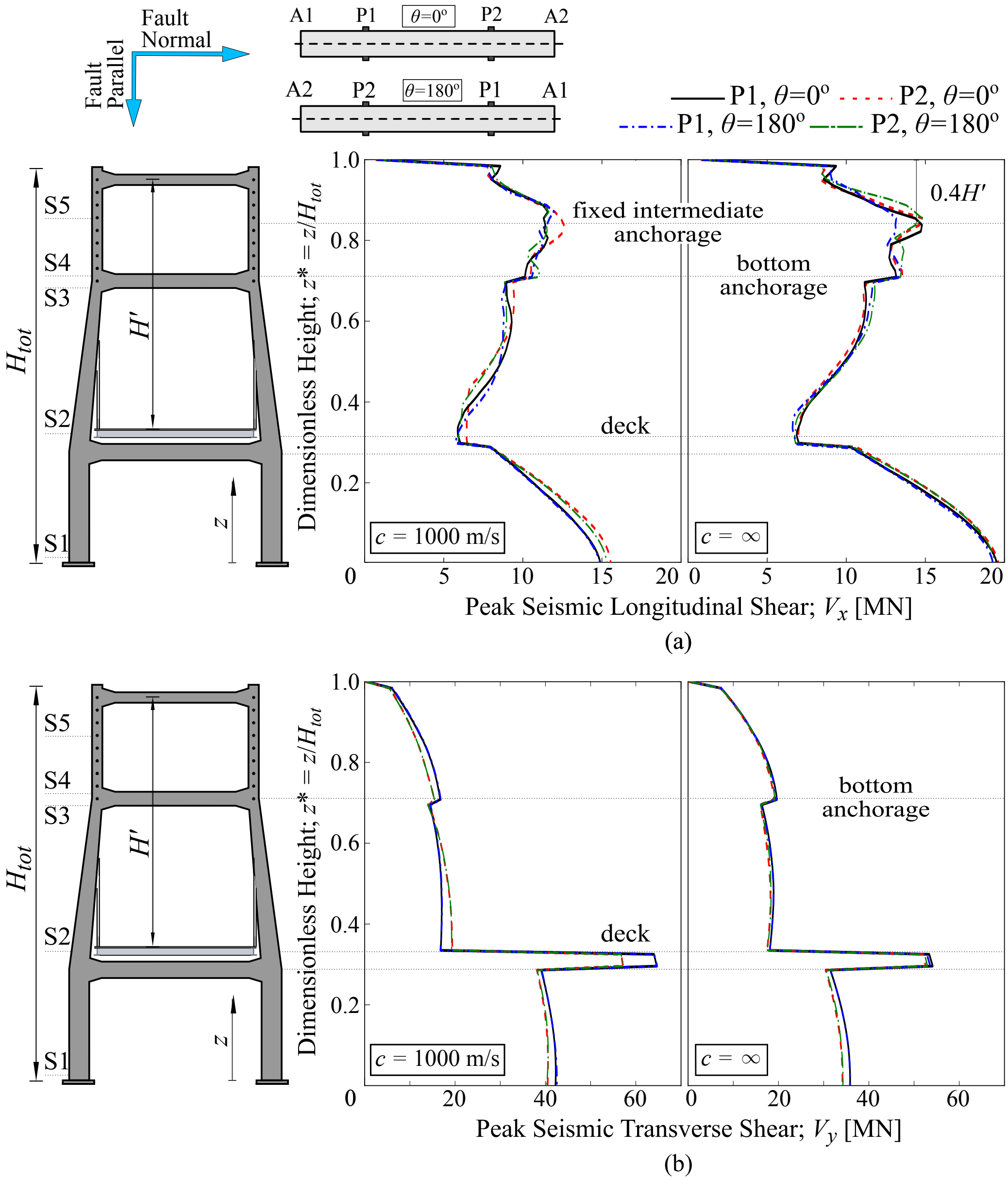

Figure 9: Mean peak seismic (a) longitudinal (V_x) and, (b) transverse (V_y) shear forces along the height of pylons P1 and P2. H-LCP bridge; $L_P = 400$ m.

direction and under the SVGM in the anchorage system, as shown in Fig. 9(a). This is attributed to the effect of the cable system transferring the longitudinal shear forces from the asynchronous motion (SVGM) of the supports from one pylon to the opposite. This effect increases with the restraint of the cable system to the relative (out-of-phase) longitudinal movement between the pylons, and it is maximised at the sections around the cable anchorages that connect the pylons with the vertically restrained points of the deck at the vertical piers in the side spans. At these points the error in the maximum seismic forces introduced by considering that the response is symmetric between the two pylons when $\theta = 0°$ is up to 18%. Figure 9(b) indicates that in the transverse direction the effect of the asymmetry is maximised at the deck level in the pylon, where the difference in V_y between pylons P1 and P2 is 14% when $\theta = 0°$. On the other hand, the maximum difference between the transverse seismic forces in the two pylons when the bridge is subjected to SYNC motions is negligible.

Figure 9 also allows to compare the seismic response of pylon P1 when $\theta = 0°$ to that of P2 when $\theta = 180°$. Both the longitudinal and the transverse responses (i.e. V_x and V_y, respectively) are almost identical throughout the pylon's height with the maximum difference reaching 14% in V_y at the deck. The same observation is made when comparing the response of P1 when $\theta = 0°$ to that of

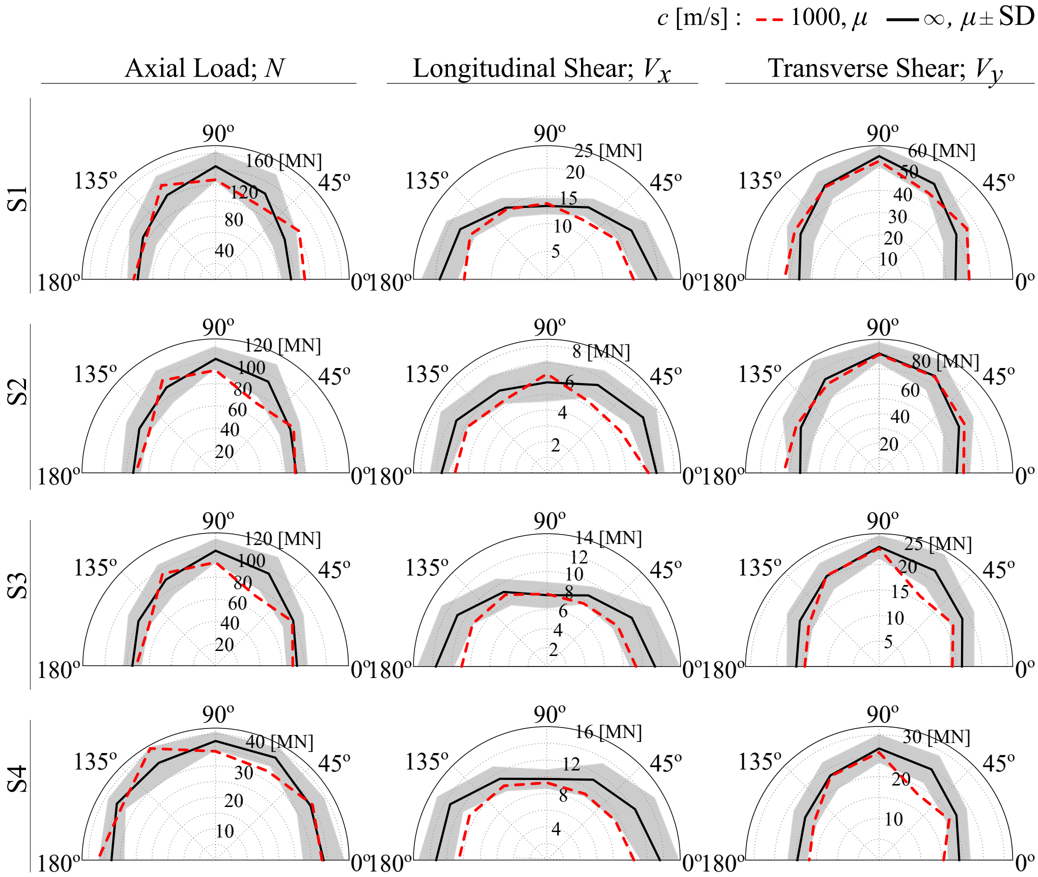

Figure 10: Peak seismic response at critical sections of the pylon for different incidence angles (θ). H-LCP model, $L_P = 400$ m.

the same pylon when $\theta = 180°$. In the longitudinal direction of the response the maximum difference of 15% is observed at the middle of the anchorage system and it is attributed to the asymmetry of the boundary conditions at the supports (Fig. 2) and to the longitudinal movement of the deck that causes alternating tension and compression between the two pylons.

In light of the results, it can be possible to consider symmetric conditions in the study of the pylons. For this reason the range of angles in which the seismic response is examined in this work is defined from $\theta = 0°$ to $180°$ hereinafter. Furthermore, because the seismic response of P2 is the largest when $\theta = 0°$ and the SVGM is considered, the results of the following sections are targeted to this one.

Critical Bridge Orientations

This section discusses the influence of the bridge orientation with respect to the propagation of the earthquake by studying the peak seismic forces in the pylon under various incidence angles (θ) of the seismic waves. These angles are considered in the range of $\theta = 0°$ to $180°$ with increments of 30°. In Fig. 10 the results are presented in the form of polar plots for the bridge with 'H'-shaped pylons and $L_P = 400$ m. These are created for the peak N, V_x and V_y at the most critical regions of the pylon starting from the base (referred to as position S1 in Fig. 9) and moving upwards to the level of the deck (position S2), to the region below the bottom cable anchorage (position S3) and to the section immediately above this (position S4). The coloured dashed line in each plot represents the arithmetic mean of the response obtained from the seven records of the set that account for the SVGM, whilst the width of the shaded band indicates two standard deviations ($\pm$SD) centred in the mean SYNC result (which is taken as the reference). Figure 10 shows that the seismic response strongly depends on the value of θ. This is mainly due to the larger spectral acceleration in the direction normal to the fault ($\mathrm{RS_{FP}} = 70\%\,\mathrm{RS_{FN}}$). The longitudinal shear force in the pylon (middle column in Fig. 10) is maximised when the strong component of the earthquake is parallel ($\theta = 0^\circ$ or 180°) to the direction of the deck. Accordingly, the transverse shear force in the pylon (right column in Fig. 10) is maximised when the strong component of the earthquake is perpendicular ($\theta = 90^\circ$) to the direction of the deck. The axial load is also maximised at $\theta = 90^\circ$ suggesting that the axial response of the pylon is dominated by the transverse flexure of the bridge. The 'H'-shaped pylons have two legs resisting the lateral movement which induces tension in one leg and compression in the other, explaining why N and V_y are maximised at the same orientation of the bridge (Efthymiou 2019). The minimum seismic response is usually obtained by rotating the earthquake by 90° from the angle in which the response is maximised, so that the minor horizontal earthquake component, i.e. the fault parallel (FP) direction, is aligned with the direction of the response under consideration. The ratio between the minimum and the maximum response for different bridge orientations is approximately 0.7, which coincides with the ratio between the spectral accelerations of FP and the FN target spectra.

The SVGM has a more pronounced effect on the longitudinal response at the base of the pylon up to the deck than on the transverse response at these sections, which generally falls within the limits of the dispersion of the results obtained from the SYNC motion in the latter direction. In the majority of the incidence angles the SVGM reduces the longitudinal shear force compared to the SYNC motion and it increases the transverse shear force at the pylon base. This increase at section S1 and S2 is due to the connection between the deck and the pylon, which releases the longitudinal movement of the deck and restrains its transverse movement, introducing out-of-phase transverse forces from the deck to the two pylons.

The difference in the values of N and V_y when $\theta = 30^\circ$ and $\theta = 120^\circ$ that is observed in the response from the SVGM is due to the time-lag and the fact that depending on the angle of incidence that is examined, the pylon under consideration receives first or second the ground motion. For example when $\theta = 30^\circ$ pylon P2 is the second one to be reached by the seismic waves, and when $\theta = 120^\circ$ P2 receives the earthquake first, as detailed in Fig. 6. When the ground motion at the two pylons is not identical (i.e. when the SVGM is considered) it can lead to differences in the response of the pylon for different values of θ.

Magnitude of the SVGM

In order to quantify the effect of the asynchronous excitation on the seismic behaviour of the bridges, the response ratio ρ_j is calculated as;

$$\rho_j = \frac{R_{\mathrm{SVGM},j}}{R_{\mathrm{SYNC},j}} \tag{16}$$

where $R_{i,j}$ with $i = \mathrm{SVGM}, \mathrm{SYNC}$ is the arithmetic mean (from the seven sets of accelerograms) of the peak response quantity under consideration: $j = V_x, V_y$. Figure 11 presents this ratio in polar form obtained from the longitudinal and the transverse shear forces at the base of pylon P2. This represents a critical region of the pylon in terms of the peak longitudinal seismic response and of the maximum effect of the SVGM in the transverse response. The ratio is presented for the H-LCP model with $L_P =$ 400 m.

The results show that the transverse response ratio, ρ_{V_y}, is larger than the longitudinal ratio, ρ_{V_x}, confirming that the effect of the SVGM at the base is more important in the transverse direction of the response. It is observed that V_x is reduced at the base of the pylon (i.e. $\rho_{V_x} < 1$) when the bridge is subjected to asynchronous motion of its supports for all incidence angles except for $\theta = 90^\circ$, where $\rho_{V_x} \simeq 1$. Therefore, it can be stated that the SVGM is beneficial for the seismic response at this region of the pylon from the point of view of the longitudinal seismic forces. On the other hand, the base

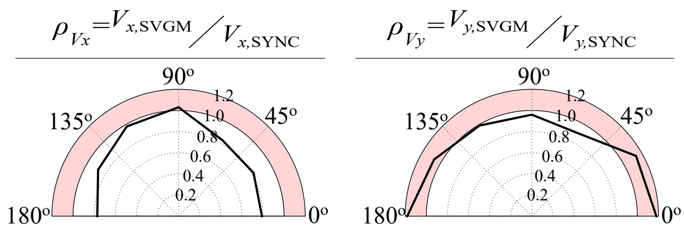

(a) (b)

Figure 11: Polar ratio ρ of the (a) longitudinal shear force (V_x) and (b) transverse shear force (V_y) at the base of the pylon (position S1) for different incidence angles (θ). $L_P = 400$ m. The coloured band denotes $\rho > 1.0$, for which the SVGM increases the seismic response.

of the pylon seems to be more vulnerable against the SVGM with ρ_{V_y} taking values of up to 1.2 when the strong earthquake component (i.e. the FN component) is parallel to the bridge ($\theta = 0°$ and $180°$). It is interesting to note the shape of the polar plots of Fig. 11 compared to the respective polar plots for the longitudinal and the transverse seismic shear forces of Fig. 10. The effect of the SVGM is minimised (in the case of ρ_{V_x}) and maximised (in the case of ρ_{V_y}) in the direction perpendicular to the one wherein the response, in terms of V_x and V_y, is maximised. This finding proves that the critical orientations of the bridge when the maximum seismic response in terms of V_x or V_y is obtained do not coincide with the orientations for which the effect of the SVGM is more significant. However, it is also found that in the case of the intermediate-span bridge ($L_P = 400$ m) the principal orientations of the bridge – the ones wherein the strong (FN) or the weak (FP) components are aligned with the deck (i.e. $\theta = 0°$, $90°$ and $180°$) – are the most important ones for the SYNC and the SVGM responses.

4.3 Influence of the Main Span Length

The discussion will focus now on the comparison between the peak seismic response along the pylons in bridges with different spans under the SVGM and the SYNC ground motion when the FN earthquake component is aligned with the deck: $\theta = 0°$. Figure 12 presents the longitudinal (top row) and the transverse (bottom row) shear forces in the legs of the pylon in the H-LCP bridge models with $L_P =$ 200, 400 and 600 m (which corresponds to pylon heights, H_{tot}, of 62.5, 125 and 187.5 m, respectively). The results show that the SVGM can reduce or increase the peak SYNC response, depending on the part of the pylon under consideration, on the length of the bridge and on the direction of the response.

Figure 12 distinguishes three regions of the pylons on which the effect of the SVGM is significant; the top part of the pylons which holds the anchorage system, the inclined part of the legs between the intermediate and the lower transverse struts, and the region below the transverse strut down to the base. It is observed that in the middle part of the inclined legs of the pylons in the 200-m span bridge the peak seismic longitudinal response is reduced by approximately 20% when the SVGM is considered (Fig. 12(a)), but the transverse response in the same region is increased by 30%. Considering the transverse response, the effect of the SVGM varies depending on the region of the pylon in which it is examined. Figure 12(b) shows that in the 400-m span bridge the SVGM reduces V_y by 25% at the level of the bottom anchorage compared to the SYNC motion, but increases it by 18% at the base of the pylon, highlighting that the effect of the SVGM depends on the region of the pylon and the direction of the response under examination.

In the longitudinal direction the effect of the SVGM generally reduces the seismic response of the pylon compared to the SYNC motion, as shown in Fig. 12(a), regardless of L_P. The influence of the SVGM is not significant in the transverse response of the pylons above the deck level (Fig. 12(b)) because the cable system hardly restrains the lateral movement of the pylons. Above the deck, the pylons can oscillate asynchronously without the development of significant forces under

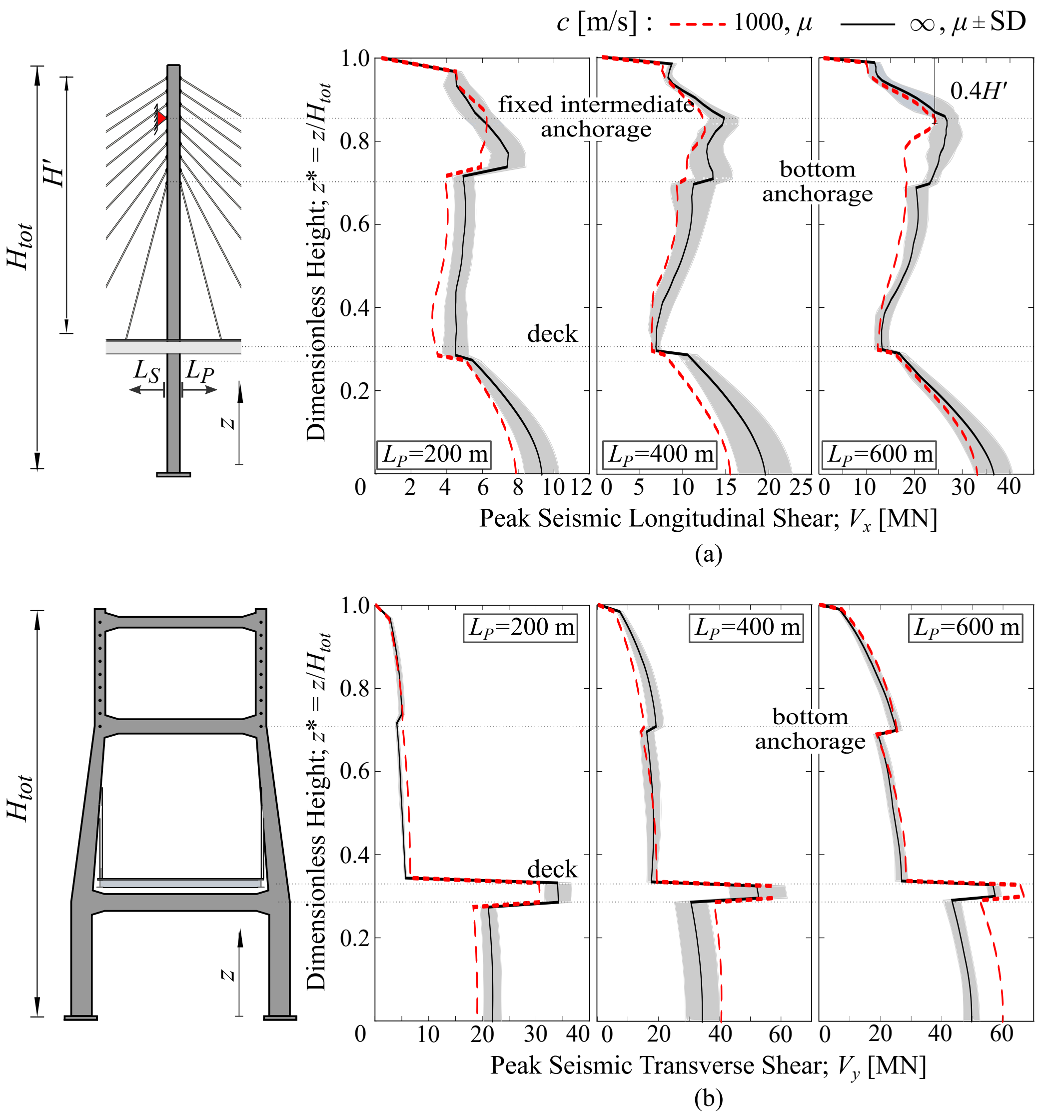

Figure 12: Effect of the SVGM for different main span lengths (L_P) on the peak seismic response of pylon P2: (a) longitudinal shear force V_x, (b) transverse shear force V_y. H-LCP model; $\theta = 0°$.

the SVGM excitation, leading to a response that is similar to the SYNC motion in terms of seismic forces. However, the effect of the SVGM in the transverse direction can be relevant at the connection between the deck and the pylons down to the base where the increment of the transverse shear is observed. This is due to the constraint between the deck and the pylons through the rigid transverse connection between them, and it is also due to the larger sections of the legs at the base compared to the intermediate and top segments of the legs (Camara *et al.* 2014). Due to the lateral restraint of the pylon movement provided by the deck, the deck-pylon reaction increases up to 20% in the 600-m span H-LCP bridge when subjected to the SVGM, which is responsible for the larger seismic forces that are observed below the bottom transverse strut of the 'H'-shaped pylon. The increasing influence of the SVGM is noticed in the transverse response of the short- and intermediate-span bridges with $L_P = 200$ and 400 m, respectively and it can be attributed to the increased influence of the vibration modes that couple the transverse flexure of the pylons and the deck, which are of increasing order as the main span increases (Camara and Efthymiou 2016).

The increase in the height of the pylons that results from the increase in the main span length $\left(H = {}^{L_P}\!/4.8\right)$ is not directly associated with the effect of the SVGM, as the current codes of practice imply by associating the effect of the SVGM to the length of the bridge (Eurocode 8; Part 1 2004). Specifically, the transverse shear from the SVGM at the level of the bottom anchorage is increased by

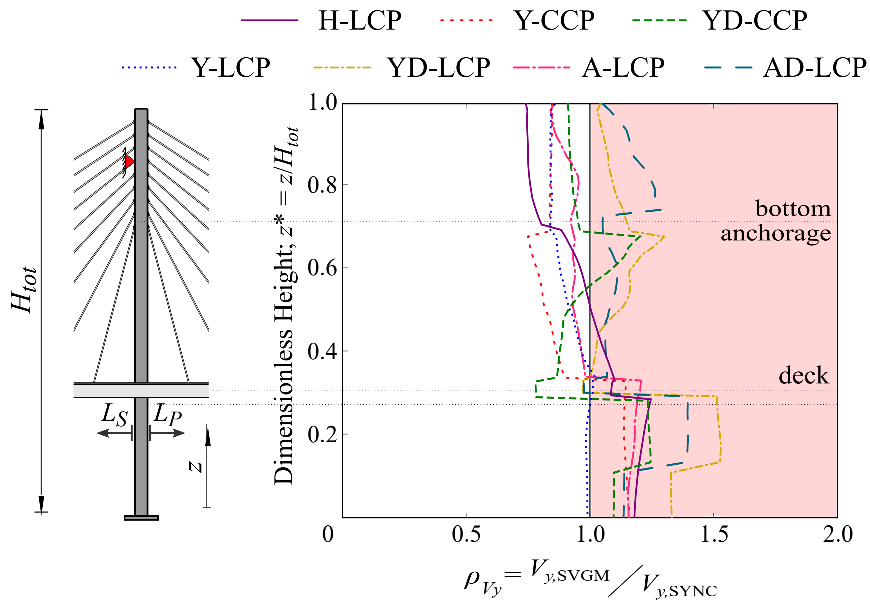

Figure 13: Transverse response ratio ρ_{V_y} along the height the of pylon. L_P = 400 m, $\theta = 0°$. The coloured band denotes $\rho_{V_y} > 1.0$, for which the SVGM increases the seismic response.

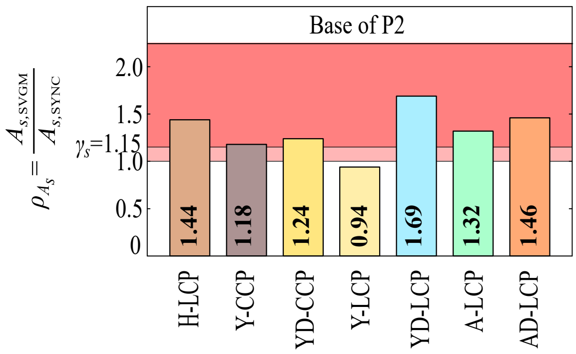

Figure 14: Variations in the required longitudinal reinforcement, A_s, from the SVGM compared to the SYNC motion at the base of the seven pylon configurations when L_P = 400 m by means of ratio ρ_{A_s}. The light and dark coloured bands denote slight and large increase in the reinforcement from the SVGM compared to the SYNC motion, respectively.

25% and reduced by 25% from the shear force from the SYNC motion in the bridges with L_P = 200 and 400 m, respectively and it is similar for both ground motion scenarios in the 600-m span bridge. On the other hand, the effect of the SVGM is larger at the base of the longest bridge compared to its intermediate-span and shortest counterparts and this is due to the largest sections of the pylons with increasing height, making them stiffer and hence, more susceptible to the multi-support excitation.

4.4 Influence of the Pylon Shape

The aim of this section is to explore how the geometry of the pylons affects the response of cable-stayed bridges that are subjected to multi-support excitations. Given that the differences between pylon geometries are mostly relevant in the direction perpendicular to the deck, the transverse magnitude of the SVGM (ρ_{V_y}) is considered as the basis for the discussion in this section.

Figure 13 shows the transverse response ratio, ρ_{V_y}, along the height of the pylons with different shapes. In general the effect of the SVGM on the seismic response varies with the pylon shape and with the region of the pylon that is examined. However, the SVGM is detrimental for the transverse response of the pylons below the deck level down to their base regardless of the pylon shape, with ρ_{V_y}

ranging from 1.1 to 1.5 due to the transverse force exerted by the deck. The exception is the lower part of the Y-LCP model in which the SVGM and the SYNC motion result in the same transverse shear force ($\rho_{V_y} \simeq 1$). Interestingly, the minimum value of ρ_{V_y} is observed in the Y-LCP model and the maximum value of ρ_{V_y} occurs in bridges with the same pylon shape above the deck but with a lower diamond configuration that connects the lateral legs of the pylons in a single vertical pier below the lower strut (YD-LCP model). This is attributed to the change in the inclination of the individual legs below the deck in the YD-LCP bridge (Fig. 1(d), (e)).

At the intermediate part of the legs, between the deck level and the anchorage of the bottom cable, only the pylons with lower diamonds have increased V_y from the SVGM compared to the respective shear force from the SYNC motion of the supports. These pylons are of inverted 'Y' and 'A' shapes (i.e. YD-CCP, YD-LCP and AD-LCP models) and they have in common the high inclination of their intermediate legs, which is reversed below the deck until they are connected to the common vertical member at the bottom (Fig. 1(c), (e) and (g)). On the other hand, the intermediate part of the Y-CCP, Y-LCP and A-LCP models, whose individual legs have constant inclination along their length, is not vulnerable to the SVGM (i.e. $\rho_{V_x} < 1$ between the bottom anchorage and the deck).

Generally, the pylons with two individual legs throughout their height are better candidates to resist the SVGM compared to the ones with lower diamonds. The SVGM increases the transverse displacement at the top of the YD-LCP pylon by 45% from the SYNC motion, whereas in the Y-LCP model the transverse displacement from the SVGM is 5% smaller than that from the SYNC motion. Similarly, in the 'A'-shaped pylons with and without lower diamonds there is an increase of 37% and 6%, respectively in the transverse displacement at the top when the pylons oscillate out-of phase compared to the SYNC motion. Figure 14 presents the variation in the required longitudinal reinforcement, A_s, from the SVGM compared to the SYNC motion at the base of the different pylons by means of the ratio ρ_{A_s}. It is observed that the large transverse displacements in the pylons under the SVGM are also reflected in the required longitudinal reinforcement at the base sections of the pylons of the YD-LCP and AD-LCP bridges with $L_P = 400$ m when subjected to multi-support excitations, which is increased by 69% and 46%, respectively from the required reinforcement when SYNC motion of the supports is considered, as shown in Fig. 14. On the other hand, a smaller increase is observed at the base of the respective pylons without lower diamonds where the required reinforcement resulting from the SVGM is 6% less and 32% more in the Y-LCP and A-LCP models, respectively compared to the SYNC motion. However, in all pylon configurations, with the exception of the Y-LCP pylon, the base section is significantly affected by the SVGM resulting in greater reinforcement ratios than the SYNC motion. These cannot be accommodated by the steel safety factor $\gamma_s = 1.15$, as defined in Eurocode 2; Part 1.1 (2004) and therefore it is verified that the SVGM needs to be considered in the design of cable-stayed bridges particularly with pylons including lower diamond configurations.

4.5 Effect of the Cable System and its Configuration

The peak seismic response of the 400-m span bridge with inverted 'Y'-shaped pylons is compared in Fig. 15 for central and lateral cable systems (CCP and LCP, respectively). It should be noted that due to the influence of the cable arrangement on the cross-section of the deck, the latter is 1.25 - 1.3% stiffer and 12.5% heavier in the bridge with one CCP and 400 m span, in comparison to the homologue LCP structure. Figure 2(d) shows the differences between the decks of the CCP and LCP bridge. However, Fig. 13 shows that the changes in the stiffness and the mass of the deck cannot explain by themselves the increased effect of the SVGM in the lower part of pylon of the CCP model, which reaches 17% in terms of the transverse response ratio. On the other hand, the effect of the cable system on this response quantity is minimised at the anchorage area of the pylon, where the ρ_{V_y} is identical between the two models. Figure 15 shows that when SYNC motion is considered the Y-CCP bridge with $L_P = 400$ m maximises the transverse deck-pylon reaction, which is 10% larger than the

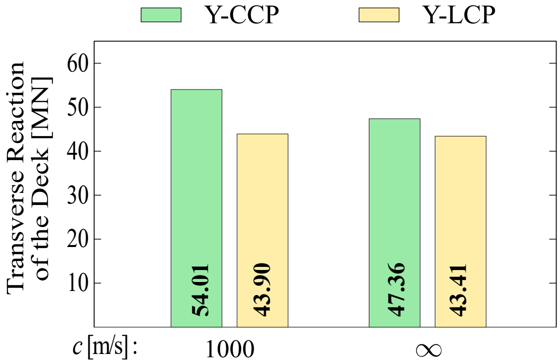

Figure 15: Peak transverse seismic reaction of the deck to the pylons legs in the Y-CCP and Y-LCP models for the SVGM ($c = 1000$ m/s) and for the SYNC motion case ($c = \infty$). $L_P = 400$ m, $\theta = 0°$.

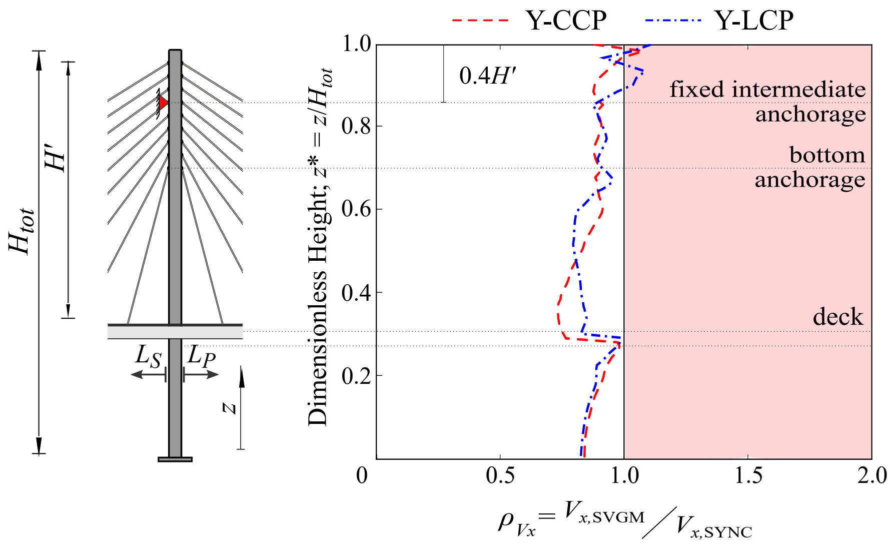

Figure 16: Longitudinal response ratio ρ_{V_x} in the pylon of the Y-CCP and Y-LCP models. $L_P = 400$ m, $\theta = 0°$. The coloured band denotes $\rho_{V_x} > 1.0$, for which the SVGM increases the seismic response.

one in the Y-LCP bridge and it is mainly attributed to the 12.5% increment in the weight of the deck. This difference is increased to 24% when the pylons move asynchronously in the transverse direction under the SVGM.

The influence of the cable-system is less significant in the longitudinal direction (ρ_{V_x}) in which the SVGM reduces the seismic response along the pylon when $\theta = 0°$ and the longitudinal component of the earthquake is maximised (i.e. FN // deck). The exception is at the top part of the cable system above the intermediate anchorage in the CCP and LCP models, as can be seen in Fig. 16, where the SVGM slightly increases V_x compared to the response from the SYNC motion by 10% ($\rho_{V_x} = 1.1$), concluding that the effect of the cable system in the response from the SVGM is more significant in the transverse direction, i.e. $\rho_{V_y} > \rho_{V_x}$. This is explained by the different configuration of the cable anchorages along the deck in CCP and LCP bridges. When the bridge has a single CCP the cables are perpendicular to the deck and the transverse seismic loads coming from the girder are concentrated to the deck-pylon connection. However, in LCP bridges the two cable planes are anchored at the edges of the deck and an additional path is provided through the inclined cable system to transmit the transverse deck loads to the pylons.

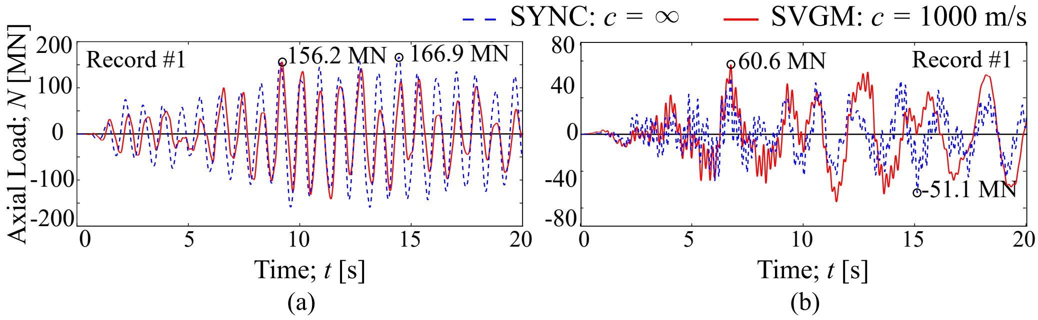

Figure 17: Response time-history of the seismic axial force (N) at the base of pylon P2 in models: (a) Y-CCP, (b) YD-CCP. Earthquake record #1, $\theta = 0°$, $L_P = 400$ m. The peak responses are annotated.

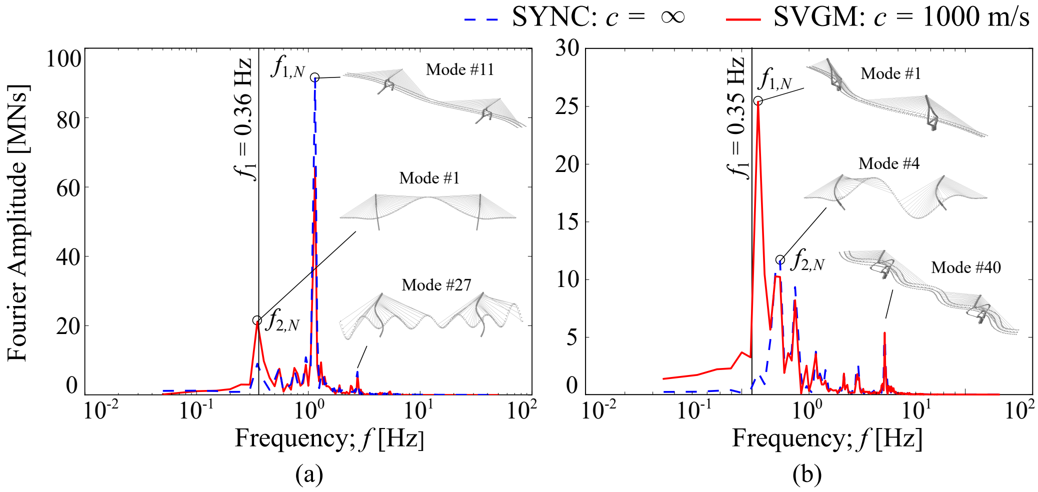

Figure 18: Frequency content of the seismic axial load (N) at the base of pylon P2 in models: (a) Y-CCP, (b) YD-CCP. Record #1, $\theta = 0°$, $L_P = 400$ m.

4.6 Modal Contribution to the Seismic Response

In this section the effect of the multi-support excitation on the frequency content of the pylons' vibration is explored. In order to examine the participation of different modes to the seismic response, the time-histories of the axial load and of the longitudinal and the transverse shear forces at the base of the pylons during the earthquakes (removing the contribution of the permanent loads) have been studied. Figure 17 compares the response time-histories of the axial force at the base of pylon P2 (position S1) from the SVGM and from the SYNC motion in the bridges with a central cable system with or without the lower diamond configuration (i.e. Y-CCP and YD-CCP).

The difference in the response of different pylons under the SVGM can be explained by the changes in the contribution of certain vibration modes. The relatively close spacing between consecutive peaks in the response time-history of the axial load from the SVGM at the base of the pylon with a lower diamond in Fig. 17(b) indicates that the response is dominated by higher-order vibration modes compared to those contributing to the axial response of the pylon without a lower diamond. According to previous studies on the seismic response of cable-stayed bridges under SYNC motion, the mode that governs the axial load in the pylon involves the vertical deformation of the lateral legs, which are especially stiff in the lower diamond pylons due to the dimensions of the vertical pier below the deck (Camara 2011). However, when the ground motion is asynchronous the axial response in the pylons with lower diamonds is dominated by a low-order vibration mode, as shown in Fig. 17(b). This is observed for all the records but only in bridges with lower diamonds. The effect is further explored in Fig. 18, which presents the frequency content of the response time-history included in Fig. 17 for earthquake record #1 by means of the fast Fourier transform (FFT). The FFT shows

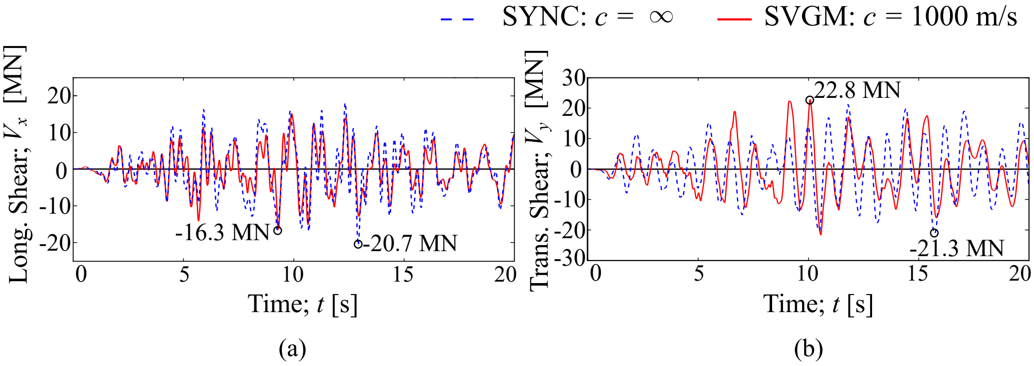

Figure 19: Response time-history of (a) the longitudinal (V_x) and (b) the transverse (V_y) shear forces at the base of pylon P2 in the Y-CCP bridge. Record #1, $\theta = 0°$, $L_P = 400$ m. The peak responses are annotated.

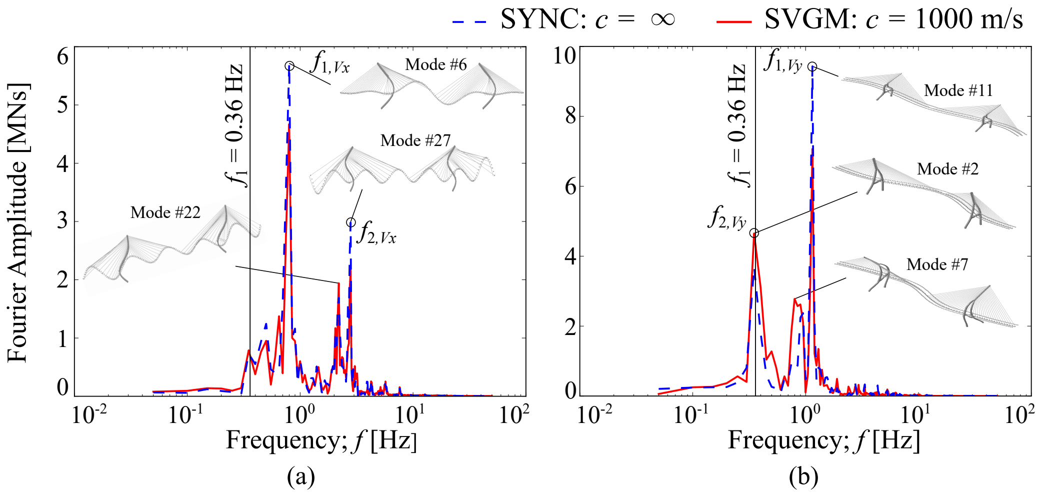

Figure 20: Frequency content of: (a) longitudinal shear force (V_x), (b) transverse shear force (V_y). Results at the base of pylon P2 in the Y-CCP model. Record #1, $\theta = 0°$, $L_P = 400$ m.

that in the 400-m span YD-CCP bridge under the SVGM the contribution to the axial response of the fundamental mode (f_1), which involves the transverse flexure of the deck, increases significantly and becomes dominant: $f_{1,N} = f_1 = 0.35$ Hz in Fig. 18(b) (where $f_{1,j}$ represents the dominant mode in the response j, with $j = N, V_x, V_y$). This mode is responsible for the low-frequency oscillation observed in the time-history illustrated in Fig. 17(b). However, the frequency content of the axial response of the bridge with inverted 'Y'-shaped pylons without lower diamonds from the SYNC motion and the SVGM is dominated by the higher transverse mode #11 of the pylons, as shown in Fig. 18(a). This happens because inverted 'Y'-shaped pylons without lower diamonds are very stiff in the transverse direction due to the constraint provided by the connection of the two lateral legs above the deck and the large inclination of their legs (Camara and Efthymiou 2016). The main difference with the YD-CCP model is that the pylons with lower diamonds have certain rotation capacity at the connection between the lateral legs and the vertical pier below the deck, which helps to accommodate the differential pylon movements in the transverse direction. This effect ultimately reduces (by up to 60%) the peak axial load in the pylon of the YD-CCP bridge in comparison to that of the Y-CCP bridge when the SVGM is considered.

By exploring the shapes of important vibration modes included in Fig. 18 it is observed that the axial response of both bridges under SYNC motion is significantly affected by longitudinal and transverse modes in which the movement of the pylons occurs in the same direction (longitudinal or transverse). This is the case of Modes #11 and #27 in the Y-CCP bridge and of modes #1, #4 and #40 in the YD-CCP model. However under the SVGM, modes with opposite movement of the pylons, and usually lower frequencies, gain importance. This is the case of mode #1 (fundamental vertical mode with opposite longitudinal movement of the pylons) in the YD-CCP bridge. This result confirms that the SYNC motion excites symmetric modes in symmetric cable-stayed bridges, whereas the SVGM also excites antisymmetric modes, which was first pointed out by Zerva (1990) in multi-span beams.

It has been observed here that the axial force in the pylons is affected by the longitudinal and the transverse response of the bridge. The discussion will now focus on the longitudinal and the transverse shear forces at the base of the pylon in order to isolate the response of the bridge in each of the two principal directions. Figure 19 shows the evolution of the longitudinal and the transverse shear forces at the base of pylon P2 during earthquake #1 in the two CCP models. The response time-history suggests that the longitudinal shear force is governed by vibration modes with higher frequencies than the transverse response, which is confirmed in the corresponding frequency content of the response presented in Fig. 20. It is also observed that the shear forces in both directions (and the corresponding bending moments) induced by the SVGM in the pylons are dominated by the same frequencies as the ones observed under the SYNC motion: $f_{1,V_x} = 0.78$ Hz being the dominant vibration frequency in the longitudinal direction (Fig. 20(a)), and $f_{1,V_y} = 1.14$ Hz for the transverse one (Fig. 20(b)). Nevertheless, the contribution of these frequencies to the total response changes under the SVGM. Figure 20(b) shows that the asynchronous motion of the pylons reduces the presence of the dominant vibration mode in the transverse response of the pylon (f_{1,V_y}). This figure also highlights that the antisymmetric mode #7 ($f_7 = 0.81$ Hz) has a significant contribution to the transverse response of the bridge under the SVGM, as opposed to the SYNC motion in which it is de-amplified. This is explained by the opposite movement of the pylons in mode #7. On the other hand, the longitudinal shear force at the pylon base is smaller under the SVGM because the contribution of the dominant vibration modes #6 ($f_6 = 0.78$ Hz) and #27 ($f_{27} = 2.72$ Hz) is reduced.

5 Conclusions

This paper has examined the effect of the SVGM on the elastic seismic response of the pylons of cable-stayed bridges. In order to obtain a general view of the problem, seven different pylon-cable system configurations and three main span lengths (L_P) of 200, 400 and 600 m have been considered. A number of increments of the seismic incidence angle with respect to the bridge axis have been examined, combined with the effect of the SVGM introduced by means of a semi-empirical loss of coherency model (Harichandran and Vanmarcke 1986) and by the time-lag of the arrival of the earthquake at different supports (wave propagation velocity is $c = 1000$ m/s). The main conclusions of this work are summarised in the following:

1. The assumption of uniform sites at the abutments and pylons of the bridges, corresponding to ground categories A and D of Eurocode 8; Part 1 (2004), is associated with the lowest and the highest seismic responses in the pylon, respectively. The increments in the response are due to the higher spectral acceleration that is associated with dominant vibration modes of the structures when ground type D is considered compared to the respective accelerations of the ground type A spectrum. When nonuniform ground conditions are considered, the seismic response generally falls within the limits defined by the uniform site conditions. Moreover, when the site response effect is combined with the incoherence and wave passage effects (i.e. the three components of the SVGM) the vertical, longitudinal and transverse response of the pylons, in almost all their height, is larger than their response when the site response effect is considered alone.
2. The effect of the SVGM varies depending on the response quantity of interest and the region of the pylons in which it is considered. The asynchronous motion generally reduces the longitudinal (parallel to the deck axis) seismic response of the pylon with the exception of the anchorage region where it is increased. This is due to the restraint provided by the cables to the

longitudinal out-of-phase oscillation of the pylons. In the transverse direction the asynchronous oscillation of the pylons above the deck level is relatively unconstrained by the cables and the girder. However, the reaction of the deck to the pylons when the latter oscillate asynchronously can increase considerably their transverse seismic response.

3. The angle of incidence of the ground motion with respect to the bridge axis, θ, is an important factor in the assessment of the seismic response of the pylons. The longitudinal shear forces in the pylon are maximised when the deck is parallel to the strong component of the ground motion (which usually corresponds to the Fault Normal orientation), whereas the transverse shear forces are maximised if the deck is perpendicular to this component (i.e. Fault Parallel // deck). The maximum effect of the SVGM on the seismic response is usually observed in the Fault Normal or Fault Parallel cases but it does not coincide with the directions of the maximum response. It can be concluded that the full assessment of the seismic response of a cable-stayed bridge requires several orientations of the deck with respect to the earthquake propagation and these should include at least the principal orientations ($\theta = 0^\circ$ and 90°), in which one of the two earthquake components are aligned with the deck, or the range of orientations from 0° to 180° for a more complete assessment.
4. The overall dimensions of the bridge influence the effect of the SVGM on the pylon but increasing the span length is not directly associated with larger effect from the SVGM. The asynchronous excitation typically increases the seismic response in the stiffer regions of the pylons which are, in turn, affected by their overall size and by the dimensions of their sections. In longer bridges (400 and 600 m spans) the effect of the SVGM tends to be more pronounced at the bottom part of the pylon from the deck down to the base. The increasing dimensions of this part of the pylons with increasing height, makes it more vulnerable against the pseudo-static forces introduced by the differential movement of the supports.
5. The pylon-cable system configuration is an important factor in the assessment of the SVGM. Bridges with a central cable plane tend to maximise the effect of the asynchronous excitation at the lower part of the pylon in the transverse direction, where the pylon shape also plays an important role in the response. It is observed that pylons which feature lower diamonds are more susceptible against the multi-support excitation, mainly because of the large stiffness of the vertical pier at their base, and also due to the rotation capacity of the connection between this member and the inclined legs of the pylon below the deck, which maximises the transverse displacement of the pylon. The pylons with lower diamonds also require increased amounts of reinforcement at their base when subjected to multi-support excitations. On the other hand, the individual legs of the ‘H’-shaped pylons (H-LCP model) or the bridges with inverted ‘Y’-shaped pylons and central cable systems (Y-CCP and YD-CCP models) are found to be better candidates to accommodate the out-of-phase motion of the supports above the deck because they constitute more ‘flexible’ configurations than the other pylon-cable system configurations studied.
6. There is a close link between the effect of the asynchronous motion on the seismic response and the vibration modes of the structure. Higher-order antisymmetric vibration modes are excited by the SVGM and are de-amplified by the SYNC motion.

References

Abaqus (2018). *ABAQUS 2018. Finite elements analysis program; Providence, RI, Dassault Systèmes Simulia*.

Abdel-Ghaffar, A. (1991). Cable - stayed bridges under seismic action. In *Cable - stayed Bridges;*

Recent Developments and their Future, pages 171–192, Yokohama (Japan). Elsevier Science Ltd.

Abdel-Ghaffar, A. and Nazmy, A. (1991). 3D nonlinear seismic behavior of cable-stayed bridges. *Journal of Structural Engineering*, 117:3456–3476.

Abdel-Ghaffar, A. and Rubin, L. (1983). Lateral earthquake response of suspension bridges. *Journal of Structural Engineering*, 109:664–675.

Allam, S. and Datta, T. (2004). Seismic response of a cable-stayed bridge deck under multi-component non-stationary random ground motion. *Earthquake Engineering & Structural Dynamics*, 33:375–393.

Amin, M. and Ang, A.-S. (1966). A nonstationary stochastic model for strong-motion earthquakes. Technical report, Structural Research Series No. 306, University of Illinois, Department oF Civil Engineering.

Ates, S., Bayraktar, A., and Dumanoglu, A. (2006). The effect of spatially varying earthquake ground motions on the stochastic response of bridges isolated with friction pendulum systems. *Soil Dynamics and Earthquake Engineering*, 26:31–44.

Bi, K., Hao, H., and Ren, W. (2010). Response of a frame structure on a canyon site to spatially varying ground motions. *Structural Engineering and Mechanics*, 36:111–127.

Burdette, N., Elnashai, A., Lupoi, A., and Sextos, A. (2006). The effect of asynchronous earthquake motion on complex bridges. Technical report, Mid-America earthquake center, Department of civil engineering, University of Illinois at Urbana-Champaign.

Camara, A. (2011). *Seismic behaviour of cable-stayed bridges: Design, analysis and seismic devices*. PhD thesis, Universidad Politécnica de Madrid, Spain.

Camara, A., Astiz, M., and Ye, A. (2014). Fundamental mode estimation for modern cable-stayed bridges considering the tower flexibility. *Journal of Bridge Engineering*, 19.

Camara, A. and Efthymiou, E. (2016). Deck-tower interaction in the transverse seismic response of cable-stayed bridges and optimum configurations. *Engineering Structures*, 124:494–506.

Chen, M.-T. and Harichandran, R. (2001). Response of an earth dam to spatially varying earthquake ground motion. *Journal of Engineering Mechanics*, 127:932–939.

Chopra, A. (2017). *Dynamics of structures, theory and applications to earthquake engineering. Fifth edition*. Pearson Education, Prentice Hall, University of California, Berkeley.

Demirci, C., Málaga-Chuquitaype, C., and Macorini, L. (2018). Seismic drift demands in multi-storey cross-laminated timber buildings. *Earthquake Engineering & Structural Dynamics*, 47:1014–1031.

Deodatis, G. (1996). Non-stationary stochastic vector processes: seismic ground motion applications. *Probabilistic Engineering Mechanics*, 11:149–168.

Der Kiureghian, A. (1996). A coherency model for spatially varying ground motions. *Earthquake Engineering & Structural Dynamics*, 25:99–111.

Der Kiureghian, A. and Neuenhofer, A. (1992). Response spectrum method for multi support seismic excitations. *Earthquake Engineering & Structural Dynamics*, 21:713–740.

Efthymiou, E. (2019). *The effect of multi-angle spatially variable ground motions on the seismic behaviour of cable-stayed bridges*. PhD thesis, City, University of London.

Efthymiou, E. and Camara, A. (2015). Spatial variability effects of the seismic action in cable-stayed bridges and modelling techniques. In *IABSE Conference – Structural Engineering: Providing Solutions to Global Challenges*, Geneva (Switzerland).

Efthymiou, E. and Camara, A. (2017). Effect of spatial variability of earthquakes on cable-stayed bridges. *Procedia Engineering*, 199:2949–2954.

Eurocode 2; Part 1.1 (2004). *Eurocode 2: Design of concrete structures. Part 1.1: General rules and rules for buildings*. EN 1992-1-1:2004.

Eurocode 3; Part 1.1 (2005). *Eurocode 3: Design of steel structures. Part 1.1: General rules and rules for buildings*. EN 1993-1-1:2005.

Eurocode 3; Part 1.11 (2006). *Eurocode 3: Design of steel structures. Part 1.11: Design of structures with tension components*. EN 1993-1-11:2006.

Eurocode 8; Part 1 (2004). *Eurocode 8: Design of structures for earthquake resistance. Part 1: General rules, seismic actions and rules for buildings*. EN 1998-1:2004.

Eurocode 8; Part 2 (2005). *Eurocode 8: Design of structures for earthquake resistance. Part 2: Bridges*. EN 1998-2:2005.

Gazetas, G. (1991). Formulas and charts for impedances of surface and embedded foundations. *Journal of Geotechnical Engineering*, 117(9):1363–1381.

Hao, H. (1997). Pipeline response to random ground motion. *Stability of simple beam subjected to multiple seismic excitations*, 123:739–742.

Hao, H., Oliveira, C., and Penzien, J. (1989). Multiple-station ground motion processing and simulation based om SMART-1 array data. *Nuclear Engineering and Design*, 111:293–310.

Harichandran, R. and Vanmarcke, E. (1986). Stochastic variation of earthquake ground motion in space and time. *Journal of Engineering Mechanics*, 112:154–174.

Hindy, A. and Novak, M. (1980). Pipeline response to random ground motion. *Journal of the Engineering Mechanics Division*, 106:339–360.

Jennings, P., Housner, G., and Tsai, N. (1968). Simulated earthquake motions. Technical report, Technical Report, Earthquake Engineering Research Laboratory, California Institute of Technology.

Kawashima, K., Unjoh, S., and Tunomoto, M. (1993). Estimation of damping ratio of cable-stayed bridges for seismic design. *Journal of Structural Engineering*, 119(4):1015–1031.

Khan, R. (2012). *Earthquake-Resistant Structures – Design, Assessment and Rehabilitation*, chapter Seismic reliability analysis of cable-stayed bridges against first passage failure. INTECH Open Access Publisher.

Lee, M. and Penzien, J. (1983). Stochastic analysis of structures and piping systems subjected to stationary support excitations. *Earthquake Engineering & Structural Dynamics*, 11:91–110.

Lopez, O., Hernandez, J., Bonilla, R., and Fernandez, A. (2006). Response spectra for multicomponent structural analysis. *Earthquake Spectra*, 22:85–113.

Lou, L. and Zerva, A. (2004). Effects of spatially variable ground motions on the seismic response of a skewed, multi-span, RC highway bridge. *Soil Dynamics and Earthquake Engineering*, 25:729–740.

Luco, J. and Wong, H. (1986). Response of a rigid foundation to a spatially random ground motion. *Earthquake Engineering & Structural Dynamics*, 14:891–908.

Mackie, K., Cronin, K., and Nielson, B. (2011). Response sensitivity of highway bridges to randomly oriented multi-component earthquake excitation. *Journal of Earthquake Engineering*, 15:850–876.

Málaga-Chuquitaype, C. and Elghazouli, A. (2012). Inelastic displacement demands in steel structures and their relationship with earthquake frequency content parameters. *Earthquake Engineering & Structural Dynamics*, 41:831–852.

Mezouer, N., Silhadi, K., and Afra, H. (2010). Importance of spatial variability of seismic ground motion effects on long beams response. *Journal of Civil Engineering and Construction Technology*, 1:1–13.

Nazmy, A. and Abdel-Ghaffar, A. (1992). Effects of ground motion spatial variability on the response of cable-stayed bridges. *Earthquake Engineering & Structural Dynamics*, 21:1–20.

Papadopoulos, S. and Sextos, A. (2018). Anti-symmetric mode excitation and seismic response of base-isolated bridges under asynchronous input motion. *Soil Dynamics and Earthquake Engineering*.

Papadopoulos, S., Sextos, A., Kwon, O., Gerasimidis, S., and Deodatis, G. (2017). Impact of spatial variability of earthquake ground motion on seismic demand to natural gas transmission pipelines. In *Proccedings of the 16th World Conference on Earthquake, 16WCEE 2017*, Santiago, Chile.

Priestley, M., Seible, F., and Calvi, G. (1996). *Seismic design and retrofit of bridges*. John Wiley & Sons Ltd.

Priestley, M. B. (1965). Evolutionary spectra and non-stationary processes. *J. Royal Statistical Society*, 27(2):204–237.

Sextos, A. (2001). *Effect of spatial variability of seismic motion, local site conditions and soil-structure interaction dynamic analysis of RC bridges*. PhD thesis, Aristotle University Thessaloniki, Greece.

Sextos, A. and Kappos, A. (2008). Asynchronous seismic excitation practice (*in greek*). In *3rd Panhellenic Conference on Earthquake Engineering and Engineering Seismology*, Athens (Greece).

Sextos, A. and Kappos, A. (2009). Evaluation of seismic response of bridges under asynchronous excitation and comparisons with Eurocode 8-2 provisions. *Bulletin of Earthquake Engineering*, 7:519–545.

Sextos, A., Kappos, A., and Mergos, P. (2004). Effect of soil-structure interaction and spatial variability of ground motions on irregular bridges: The case of the Krystallopigi Bridge. In *13th World Conference on Earthquake Engineering*, Vancouver (B.C. Canada).

Sextos, A., Karakostas, C., Lekidis, V., and Papadopoulos, S. (2014). Multiple support seismic excitation of the Evripos Bridge based on free-field and on-structure recordings. *Structure and Infrastructure Engineering*, 11:1510–1523.

Sextos, A., Pitilakis, K., and Kappos, A. (2003). Inelastic dynamic analysis of RC bridges accounting for spatial variability of ground motion, site effects and soil–structure interaction phenomena. Part 1: Methodology and analytical tools. *Earthquake Engineering & Structural Dynamics*, 32(4):607–627.

Shinozuka, M. (1972). Monte Carlo solution of structural dynamics. *Computers & Structures*, 2:855–874.

Shinozuka, M., Saxena, V., and Deodatis, G. (2000). Effect of spatial variation of ground on highway structures. Technical report, MCEER ISN 1520-295X.

Soyluk, K. and Dumanoglu, A. (2000). Comparison of asynchronous and stochastic dynamic responses of a cable-stayed bridge. *Engineering Structures*, 22:435–445.

Soyluk, K. and Dumanoglu, A. (2004). Spatial variability effects of ground motions on cable-stayed bridges. *Soil Dynamics and Earthquake Engineering*, 24:241–250.

Stefanidou, S., Sextos, A., Kotsoglou, A., Lesgidis, N., and Kappos, A. (2017). Soil-structure interaction effects in analysis of seismic fragility of bridges using an intensity-based ground motion selection procedure. *Engineering Structures*, 151:366–380.

Tzanetos, N., Elnashai, A., Hamdan, F., and Antoniou, S. (2000). Inelastic dynamic response of RC bridges subjected to spatial non-synchronous earthquake motion. *Advances in Structural Engineering*, 3:191–214.

Wang, J., Carr, A., Cooke, N., and Moss, P. (2003). Wave-passage effect on the seismic response of long bridges. In *2003 Pacific Conference on Earthquake Engineering*.

Zerva, A. (1990). Response of multi-span beams to spatially incoherent seismic ground motions. *Earthquake Engineering & Structural Dynamics*, 19:819–832.

Zerva, A. (1991). Effect of spatial variability and propagation of seismic ground motions on the response of multiply supported structures. *Probabilistic Engineering Mechanics*, 6:212–221.

Zerva, A. (2009). *Spatial variation of seismic ground motions: Modeling and engineering applications*. CRC Press, Boca Raton.